Cell proliferation assay and matrigel invasion assay

For cell proliferation assays, 4.0×10^4 cells were plated in triplicate on 24-well plates containing DMEM medium with 10% FBS, 1% antibiotics, and glutamine solution. Subsequently, the cell number was calculated using the Trypan-blue staining and an automated cell counter (TC10 Bio-Rad Laboratories, Tokyo, Japan) after transfection with siRNA for 24, 48, 72, and 96 h.

A matrigel invasion assay was performed using the Biocoat Matrigel Invasion Chamber (BD) according to the manufacturer's protocols. In brief, 4.0×10^4 cells were plated in the upper insert chamber in serum-free medium. The bottom chamber contained DMEM medium with 10% FBS as an inducer of invasion. After 48 h, the bottom of the insert chamber was fixed and stained with Diff-Quick staining (Sysmex, Kobe, Japan). Cells on the dissected stained membrane were counted under a microscope. Each membrane was divided into four quadrants and the sum of all four quadrants was calculated. Each matrigel invasion assay was performed in triplicate, and compared with migration assays using control insert membranes.

Comprehensive gene expression analysis using microarrays

Total RNAs from #1si*HOTAIR*-transfected SBC-3 cells and control cells (si*GFP*-transfected cells), were extracted using RNeasy mini kit Plus (Qiagen) and hybridized to the microarrays, Sure Print G3 Human GE 8 × 60K microarrays (Agilent Technologies, Santa Clara, CA), according to the manufacturer's instructions. Subsequently, data analysis was carried out using the GeneSpring GX 12 software (Agilent Technologies), with a stringency of $P < 0.1$ and a twofold or more change using gene ontology analysis.

Statistical analysis

Continuous datasets were compared using an independent *t*-test between two groups, and categorical datasets were analyzed by the chi-square test. Significance of difference between two or more groups was estimated with the Mann–Whitney *U*-test or the Kruskal–Wallis test, as appropriate. Disease-specific survival (DSS) was defined by death only from SCLC. Relapse-free survival (RFS) was defined by metastasis as the first recurrence event. In this study, because second primary cancers were not found in all subjects, RFS is de facto disease-free survival (DFS). DSS and RFS/DFS curves were plotted according to the Kaplan–Meier method with the Cox–Mantel log-rank test applied for comparison. Univariate and multivariate analyses by the Cox proportional hazard method were performed. All differences were considered statistically significant at the level of $P < 0.05$, and there being a tendency at a level of $P < 0.10$. SPSS 19.0 (IBM Corporation, Somers, NY) was used for statistical analyses.

Results

Clinicopathological profiles of 35 SCLC cases

We assessed 35 surgically removed SCLC tumors and 15 lung tissues. The patients were mostly male, the average age was 65.8 years, and cumulative smoking was over 50 pack-years. Nine cases undertook chemotherapy before surgery, typically four courses of platinum (cisplatin [CDDP] or carboplatin [CBDCA]) plus etoposide (VP-16), and 26 (74%) cases did not have chemotherapy. Histologically, 69% ($n = 24$) were pure SCLC and vascular invasions were often observed (83%, $n = 29$). As expected, there were many stage I cases ($n = 15$, 43%). Generally, although SCLC patients once improved after chemotherapy, relapses frequently occur, resulting in poor prognosis. During the period of observation, 43% ($n = 15$) had relapses and 46% ($n = 16$) died. DSS and RFS/DFS were 45.3 ± 35.7 months and 40.9 ± 38.5 months, respectively.

HOTAIR expressions and clinicopathological factors in SCLC

We assessed *HOTAIR* expression levels in 35 tumors and 15 normal tissues by qRT-PCR normalized to the *ACTB*. *HOTAIR* levels between tumor tissues ($n = 35$) and normal tissues ($n = 15$) were not different significantly when analyzed across all cases ($P = 0.992$ [Mann-Whitney U test]; Fig. 1A). When compared between pure-SCLC tumor tissues ($n = 24$) and combined-SCLC tumor tissues ($n = 11$), *HOTAIR* expression was significantly higher in pure SCLC ($P = 0.009$; Fig. 1B). For pure-SCLC cases, *HOTAIR* had a tendency to be expressed more in tumor tissues ($n = 24$) than normal tissues ($n = 13$) ($P = 0.092$; Fig. 1C). Since chemotherapy prior to surgery might have some effect on cellular nature, analysis was limited to cases without such treatment (pure-NAC(−) cases), resulting in significantly higher expression in tumor ($n = 18$) than normal tissues ($n = 9$) ($P = 0.012$; Fig. 1D).

We divided 35 subjects by *HOTAIR* expression into two groups: high expression ($n = 12$) and low expression ($n = 23$), according to a *HOTAIR/ACTB* ratio of 1.368 in tumor tissues, obtained by the ROC method (Fig. 2A). The high-expression group contained significantly more pure SCLC ($P = 0.04$), more lymphatic invasion

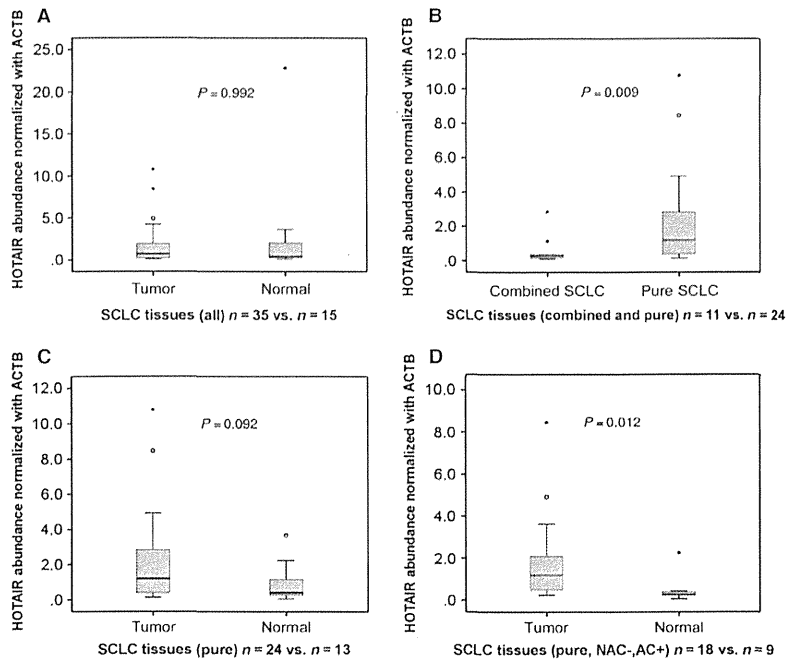

Figure 1. *HOTAIR* expression levels assessed by quantitative RT-PCR in 35 SCLC and normal tissues. Comparisons between all the tumors (n = 35) and normal tissues (n = 15) (A), pure (n = 24) and combined (n = 11) SCLC (B) (P = 0.009), pure SCLC and normal (C), and between pure SCLC with adjuvant chemotherapy and no neoadjuvant chemotherapy (n = 18) and normal (D) (P = 0.012) were made. *HOTAIR* was highly expressed in pure SCLC than combined SCLC and normal tissues.

(P = 0.03), and more relapse (P = 0.04) than the low-expression group (Table 1). To perform survival analysis, we focused only on cases with pure SCLC, without NAC and with AC (n = 8 in high-expression group and n = 10 in low-expression group). The high-expression group tended to have lower survival for RFS/DFS (P = 0.086), but not for DSS (P = 0.263) (Fig. 2B and C). Univariate analyses of DSS in all the subjects revealed that there were tendencies toward poor prognosis in the cases with relapse and pathological stages II or higher (P = 0.058, 0.099, respectively, Table S2). Multivariate analyses of DSS demonstrated that AC (P = 0.005) and pathological stages (P = 0.02) were significant prognostic factors (Table S2). However, *HOTAIR* expression was not a prognostic factor by either uni- or multivariate analyses. In regard to RFS/DFS, multivariate analyses showed that AC and pathological stages were significant prognostic factors (P = 0.004 and 0.021, respectively) and there was a tendency to poor prognosis in the cases with high-*HOTAIR* expression (P = 0.071) as indicated in Table S2.

Expression of *HOTAIR* in SCLC cells and their xenografts

We next examined *HOTAIR* expression in cell lines and normal cells. Normal cells had no expression. There were five SCLC cell lines (COR-L51, COR-L88, DMS-79, Lu-134A, and SBC-3) whose expression was significantly higher than normal, whereas the other five cell lines and the adenocarcinoma line showed the same low-level expression as normal cells. The SBC-3 cells expressed particularly highly (Fig. 3A). We made xenografts from these five cell lines and assessed *HOTAIR* expression using RT-PCR as normalized to *ACTB*. Although Lu-134A and DMS-79 lines expressed significantly highly compared with states of culture, it was SBC-3 that expressed most highly (Fig. 3B).

Consequently, we selected SBC-3 cells for further analyses. The SBC-3 line is an adherent cell line, others are not, and therefore RNAi was successful.

Depletion of *HOTAIR* by siRNA leading to decreased proliferation and invasiveness

#1–3 siRNAs against *HOTAIR* gene and si*GFP* were conformed as described [8, 9, 14]. All three siRNAs worked well and the gene expression was reduced significantly (Fig. 4A). In the proliferation experiments, however, depletion of *HOTAIR* by #1 si*HOTAIR* in SBC-3 cells dramatically decreased its proliferation ability whereas transfection of #2 or #3 si*HOTAIR* did not (Fig. 4B). Also, in the invasion assay, #1 si*HOTAIR* successfully

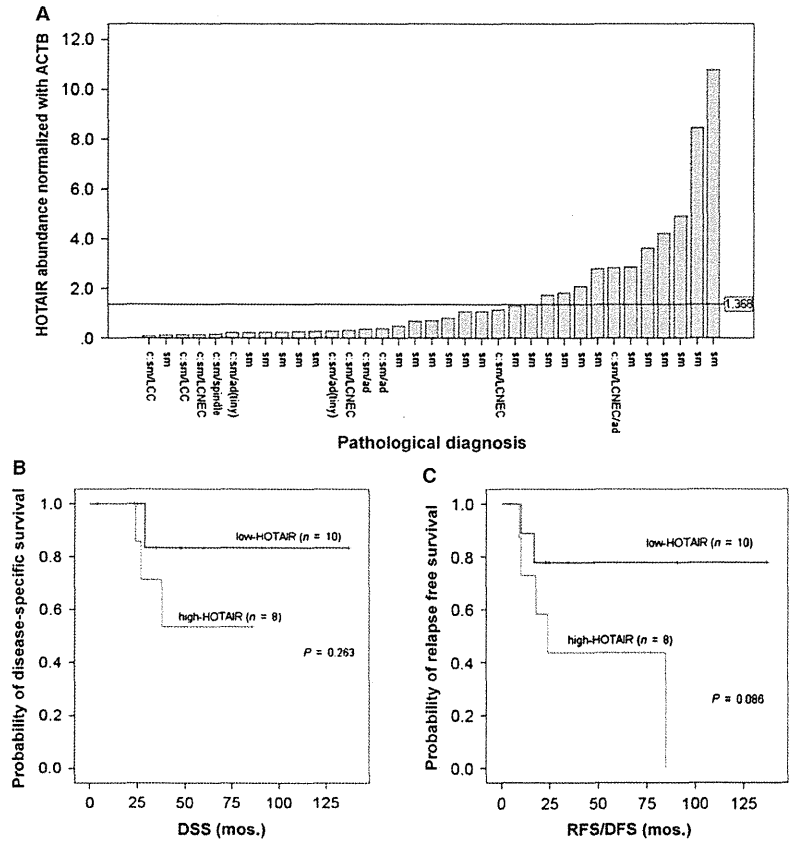

Figure 2. *HOTAIR* expression levels in SCLC and survival curves by *HOTAIR* expression. (A) *HOTAIR* expression in 35 SCLC and a reference level (*HOTAIR/ACTB* ratio = 1.368). (B and C) The Kaplan–Meier DSS curves and RFS/DFS curves, respectively, according to *HOTAIR* levels in pure-SCLC cases with adjuvant chemotherapy and no neoadjuvant chemotherapy (n = 18). Note that there was a tendency to poor prognosis in the high-expression group for the RFS/DFS of these groups (P = 0.086). For abbreviations, see text.

reduced matrix invasiveness as compared with controls (si*GFP* transfection), whereas #2–3 siRNA did not (Fig. 4C).

Gene ontology analysis in si*HOTAIR*-transfected cells

We tested whether *HOTAIR* depletion by siRNA affected the pattern of gene transcriptions, especially in genes related to proliferation and invasiveness targeted by si*HOTAIR*. We succeeded in the transfection experiments using the SBC-3 cell line and subsequently performed gene expression analysis. Raw data of two samples (#1 si*HOTAIR*-transfected cells and si*GFP*-transfected cells) were deposited in the GEO database (GSE43877). We identified significantly altered 110 genes. Ontology analyses demonstrated that many of these genes were related to cell adhesion, proliferation, and mucin formation.

Among the upregulated genes, there were those related to cell adhesion such as *ASTN1* (*astrotactin 1*), *PCDHA1* and *10* (*protocadherin-alpha* [*Pcdha*] 1 and 10), and *CLDN11* (*Claudin-11*), and genes involved in mucin production including *MUC5AC* and *MUC4*. In addition, *ECM2*, coding an extracellular matrix protein, and *NRP2*, coding a transmembrane protein interacting with vascular endothelial growth factor, were among the top 15 upregulated genes (Table S3). The top 15 downregulated genes include *NTM*, neurotrimin, encoding a protein that may promote neurite outgrowth and adhesion, *PTK2B*, *protein tyrosine kinase 2 beta* (also known as *Pyk2*), which functions in the activation of MAPK signaling pathways, and *CTNNA2*, catenin (*cadherin-associated protein*) *alpha* 2, expression of which is important for maintaining a subset of neurons. In addition, *SIRPG* (*signal regulatory protein gamma*), a member of the immunoglobulin superfamily, known to be involved in the negative regulation of receptor tyrosine kinase-coupled signaling processes, and *ITGB8* (*Integrin beta-8*), coding a member of the integrin beta chain family, are downregulated. Generally, integrin complexes mediate cell–cell and

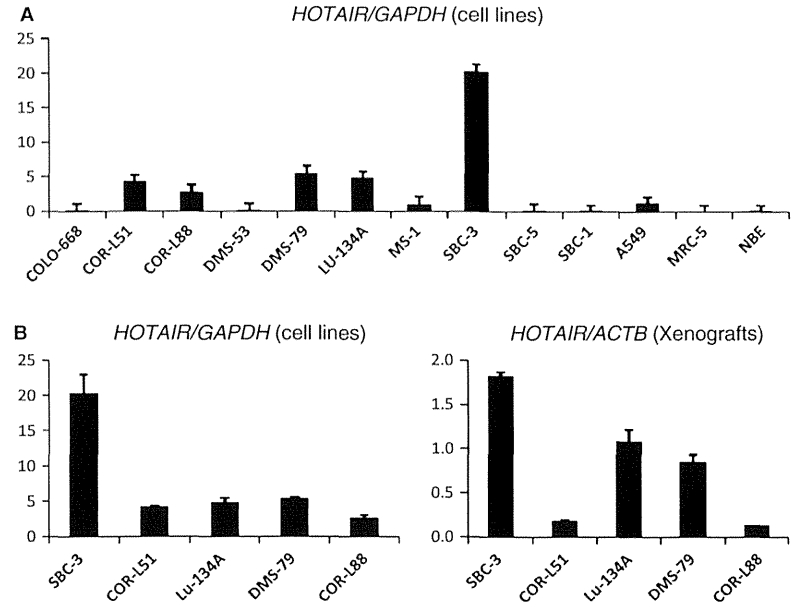

Figure 3. Expression of *HOTAIR* in cell lines and xenografts of SCLC. (A) Relative expression levels normalized to *GAPDH*. The SBC-3 line showed particularly high expression. (B) Comparisons in five SCLC cell lines with higher expression than normal cells. For abbreviations, see text.

cell–extracellular matrix interactions and play a role in human airway epithelial proliferation.

Discussion

Among lincRNAs, *HOTAIR* is one of the most remarkable because of its relevance to metastases in common cancers such as breast and colon cancers. Here, we first demonstrated that *HOTAIR* was expressed in pure SCLC and higher expression was significantly related to lymphatic invasion and relapse. Multivariate analyses demonstrated that *HOTAIR* expression correlated with RFS. In vitro experiments demonstrated that half of SCLC cell lines expressed *HOTAIR* at higher levels than normal cells and that, using SBC-3 cells, knockdown of *HOTAIR* decreased proliferative activity and cellular invasiveness with altered expression of cell adhesion-related genes.

Accumulating reports suggest that *HOTAIR* is related to poorer prognosis of tumors. Several studies have shown a relationship between high *HOTAIR* expression and the poorer prognosis of diverse cancers [14–22], but there are few studies that reveal the importance of *Hox*-related genes and/or *HOTAIR* in SCLC because of the scarcity of fresh tissue samples. In fact, almost all evidence obtained for alterations of expression in *Hox*-related genes in SCLC to date was based on cell lines and their xenografts [26–29]. To our knowledge, this is the first report on *HOTAIR* expression in primary SCLC tissues. In particular, we have shown that *HOTAIR* expression is significantly higher in SCLC tumors than normal tissues, considering induction chemotherapy (Fig. 1D), and that high expression of *HOTAIR* is relevant for relapse of SCLC. This tumor type is special for lung cancer, but proved to share similar characteristics of *HOTAIR*-related cellular regulations with ordinary carcinomas including those of breast and colon. Furthermore, our knockdown experiments of *HOTAIR* demonstrated that its depletion in SBC-3 cells caused altered expression of genes involved in neural cell adhesion, proliferation, and mucin formation although the findings are based on one cell line.

It is interesting, although not surprising, that *HOTAIR* correlates with SCLC proliferation and invasion with expression of genes implicated in cell adhesion and mucin production. In fact, depletion of *HOTAIR* upregulates genes implicated with cellular adhesion and mucin production including *ASTN1*, *PCDHA1*, and *MUC5AC*. The roles of each of these genes have been elucidated to some extant: *ASTN1*, is required for appropriate and timely migration of cerebellar granule cells [30]; *PCDHA1* belongs to the cadherin superfamily and mediate the formation and maintenance of specific synaptic connections [31]; *MUC5AC*, whose expression of protein and mRNA is significantly decreased in gastric cancer tissue [32]. On the other hand, the depletion of *HOTAIR* downregulates some genes implicated in tumor invasion and

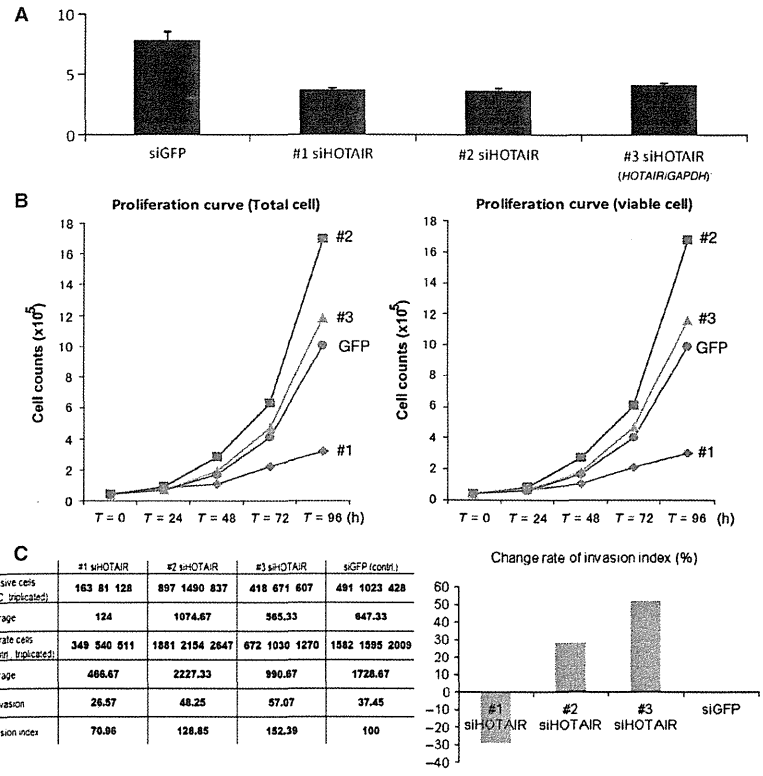

	#1 siHOTAIR	#2 siHOTAIR	#3 siHOTAIR	siGFP (contrl.)
Invasive cells (MC triplicated)	163 81 128	897 1490 837	418 671 607	491 1023 428
average	124	1074.67	565.33	647.33
Migrate cells (contrl. triplicated)	349 540 511	1881 2154 2647	672 1030 1270	1582 1595 2009
average	466.67	2227.33	990.67	1728.67
%invasion	26.57	48.25	57.07	37.45
invasion index	70.96	128.85	152.39	100

Figure 4. *HOTAIR* abundance, cellular proliferation and invasiveness in SBC-3 cells with transfection of siRNA and of siGFP. (A) The graph showed the *HOTAIR/GAPDH* ratio. #1–3 si*HOTAIR*s successfully reduced the expression levels. (B), #1 si*HOTAIR*-transfected cells reduced their ability of proliferation after 72 h, although #2, #3 si*HORAIR* did not reduce. (C) Invasiveness was assessed by % invasion and invasion index according to manufactures' protocol. In #1 si*HOTAIR*-transfected cells, almost 30% reduction of matrigel invasiveness was seen, whereas #2 and #3 si*HOTAIR* did not reduce invasiveness.

proliferation; *NTM* is expressed in fetal brain at higher levels than that in mature brain and is more highly expressed in nervous tumors than that in normal brain tissues [33]; *PTK2B* mediates cell proliferation and invasiveness in HCC cells by upregulation of the *c-Src* and ERK/MAPK-signaling pathway, and is related to progression and metastasis in breast cancer, together with focal adhesion kinase [34, 35]. Genes with fold change values of 10 or more were including genes mainly relevant to neural development (*ASTN1*, *PCDHA1*, *MUC5AC*, and *NTM*). Our data suggest that *HOTAIR* mainly regulates the expression of genes related to neural development in SCLC cells.

Possible limitations of our analysis and interpretation are as follows: First, our analyses were based on surgically resectable cases representing a very minor population. In fact, several reports indicated that patients with surgically resectable SCLC had much better prognosis and showed 5-year survival rate 30–70% [36–38], and we were not able to show significantly different survival between the groups with low- and high-*HOTAIR* expression (Fig. 2B and C). However, if we only used material from inoperable cases, in other words, the majority of SCLC patients, almost all patients were of extended disease, and as a result, we had almost no patients with good prognosis. Certainly, we need more cases with good prognosis to obtain significant difference of prognosis between low- and high-*HOTAIR* groups. Second, we succeeded in RNAi experiments using only the SBC-3 cells. As mentioned above, the SBC-3 cell line was established from a bone metastasis and not from a primary site. It is known that *HOTAIR* expression in metastatic sites was higher than in primary sites for breast cancer [14]. Possibly, high expression in the SBC-3 cells may be due to its metastatic nature, rather than its neuroendocrine nature. Further analysis using other cell lines is warranted although RNAi experiments will be a challenge.

Finally, although the knockdown efficacy was similar in #1–3 si*HOTAIR*s, suppression of cell proliferation and invasion were induced only by #1 si*HOTAIR*. This might be because the time to onset of gene silencing only by #1 siRNA was appropriate, and because the sequence

conditions of the three siRNAs were different. In particular for the latter point, following four sequence conditions were suggested to give rise to highly effective RNAi in mammalian cells [39, 40]: (1) the 5′ antisense-strand (AS) end, A or U; (2) the 5′ sense-strand (SS) end, G or C; (3) the 5′-terminal one third of AS, A/U-rich; and (4) a long G/C stretch, absent from the 5′-terminal two thirds of SS. Considering these conditions as compared among #1–3 si*HOTAIRs*, only #1 si*HOTAIR* met the four conditions at the same time.

si*HOTAIR* may represent a new therapeutic target for SCLC, in particular, of its metastatic phase. Although several kinds of pharmaceutical agents are available for SCLC treatment, *HOTAIR* therapy may be useful after the development of multidrug resistance. However, we have to bear in mind that biological, pathological, and clinical evidence for SCLC on *HOTAIR* is very limited and that our knowledge of homeobox genes, the target genes of *HOTAIR*, is very sparse. Further analysis of *HOTAIR* expression in systemic tissues of both adults and fetuses followed by further cell line experiments and in vivo analyses on tissue effects by siRNA administration using a more number of siRNA will be required.

Acknowledgments

Parts of this study were supported financially by Grants-in-Aid for Scientific Research from the Ministry of Education, Culture, Sports, Science and Technology, Japan, grants from the Japan Society for the Promotion of Science, the Ministry of Health, Labour and Welfare, and the Princess Takamatsu Cancer Research Fund. We thank Mime Kobayashi and Tamiko Minamisawa, Division of Protein Engineering, The JFCR Cancer Institute, for their help in using fluorescence microscope, and Takeshi Fujiwara, The JFCR Genome Center, for his help in using web-based databases.

Conflict of Interest

Yuichi Ishikawa is supported by research grants from SONY corporation and Daiichi-Sankyo Co. Ltd.

References

1. Field, J. K., and S. W. Duffy. 2008. Lung cancer screening: the way forward. Br. J. Cancer 99:557–562.
2. Puglisi, M., S. Dolly, A. Faria, J. S. Myerson, S. Popat, and M. E. O'Brien. 2010. Treatment options for small cell lung cancer – do we have more choice? Br. J. Cancer 102:629–638.
3. D'Angelo, S. P., and M. C. Pietanza. 2010. The molecular pathogenesis of small cell lung cancer. Cancer Biol. Ther. 10:1–10.
4. Ponting, C. P., P. L. Oliver, and W. Reik. 2009. Evolution and functions of long noncoding RNAs. Cell 136:629–641.
5. Mercer, T. R., M. E. Dinger, and J. S. Mattick. 2009. Long non-coding RNAs: insights into functions. Nat. Rev. Genet. 10:155–159.
6. Tsai, M. C., R. C. Spitale, and H. Y. Chang. 2011. Long intergenic noncoding RNAs: New links in cancer progression. Cancer Res. 71:3–7.
7. Pauli, A., J. L. Rinn, and A. F. Schier. 2011. Non-coding RNAs as regulators of embryogenesis. Nat. Rev. Genet. 12:136–149.
8. Rinn, J. L., M. Kertesz, J. K. Wang, S. L. Squazzo, X. Xu, S. A. Brugmann, et al. 2007. Functional demarcation of active and silent chromatin domains in human *Hox* loci by noncoding RNAs. Cell 129:1311–1323.
9. Tsai, M. C., O. Manor, Y. Wan, N. Mosammaparast, J. K. Wang, F. Lan, et al. 2010. Long noncoding RNA as modular scaffold of histone modification complexes. Science 329:689–693.
10. Ballas, N., C. Grunseich, D. D. Lu, J. C. Speh, and G. Mandel. 2005. REST and its corepressors mediate plasticity of neuronal gene chromatin throughout neurogenesis. Cell 121:645–657.
11. Sun, G., K. Alzayady, R. Stewart, P. Ye, S. Yang, W. Li, et al. 2010. Histone demethylase LSD1 regulates neural stem cell proliferation. Mol. Cell. Biol. 30:1997–2005.
12. Sauvageau, M., and G. Sauvageau. 2010. Polycomb group proteins: multi-faceted regulators of somatic stem cells and cancer. Cell Stem Cell 7:299–313.
13. Alves, C. P., A. S. Fonseca, B. R. Muys, E. de Barros, R. Lima Bueno, M. C. Bürger. 2013. The lincRNA Hotair is required for epithelial-to-mesenchymal transition and stemness maintenance of cancer cells lines. Stem Cells 31:2827–2832.
14. Gupta, R. A., N. Shah, K. C. Wang, J. Kim, H. M. Horlings, D. J. Wong, et al. 2010. Long non-coding RNA HOTAIR reprograms chromatin state to promote cancer metastasis. Nature 464:1071–1076.
15. Yang, Z., L. Zhou, L. M. Wu, M. C. Lai, H. Y. Xie, F. Zhang, et al. 2011. Overexpression of long non-coding RNA HOTAIR predicts tumor recurrence in hepatocellular carcinoma patients following liver transplantation. Ann. Surg. Oncol. 18:1243–1250.
16. Kogo, R., T. Shimamura, K. Mimori, K. Kawahara, S. Imoto, T. Sudo, et al. 2011. Long noncoding RNA HOTAIR regulates polycomb-dependent chromatin modification and is associated with poor prognosis in colorectal cancers. Cancer Res. 71:6320–6326.
17. Li, X., Z. Wu, Q. Mei, X. Li, M. Guo, X. Fu, et al. 2013. Long non-coding RNA HOTAIR, a driver of malignancy, predicts negative prognosis and exhibits oncogenic activity in oesophageal squamous cell carcinoma. Br. J. Cancer 109:2266–2278.

18. Tang, L., W. Zhang, B. Su, and B. Yu. 2013. Long noncoding RNA HOTAIR is associated with motility, invasion, and metastatic potential of metastatic melanoma. Biomed. Res. Int. 2013:251098.
19. Xu, Z. Y., Q. M. Yu, Y. A. Du, L. T. Yang, R. Z. Dong, L. Huang, et al. 2013. Knockdown of long non-coding RNA HOTAIR suppresses tumor invasion and reverses epithelial-mesenchymal transition in gastric cancer. Int. J. Biol. Sci. 9:587–597.
20. Lv, X. B., G. Y. Lian, H. R. Wang, E. Song, H. Yao, and M. H. Wang. 2013. Long noncoding RNA HOTAIR is a prognostic marker for esophageal squamous cell carcinoma progression and survival. PLoS ONE 8:e63516.
21. Nie, Y., X. Liu, S. Qu, E. Song, H. Zou, and C. Gong. 2013. Long non-coding RNA HOTAIR is an independent prognostic marker for nasopharyngeal carcinoma progression and survival. Cancer Sci. 104:458–464.
22. Nakagawa, T., H. Endo, M. Yokoyama, J. Abe, K. Tamai, N. Tanaka, et al. 2013. Large noncoding RNA HOTAIR enhances aggressive biological behavior and is associated with short disease-free survival in human non-small cell lung cancer. Biochem. Biophys. Res. Commun. 436:319–324.
23. Travis, W. D., E. Brambilla, H. K. Muller-Hermelink, and C. C. Harris. 2004. Pathology and genetics: tumours of the lung, pleura, thymus and heart. Vol. 1. IARC, Lyon, France, 31–34.
24. Nguewa, P. A., J. Agorreta, D. Blanco, M. D. Lozano, J. Gomez-Roman, B. A. Sanchez, et al. 2008. Identification of importin 8 (IPO8) as the most accurate reference gene for the clinicopathological analysis of lung specimens. BMC Mol. Biol. 9:103.
25. Daniel, V. C., L. Marchionni, J. S. Hierman, J. T. Rhodes, W. L. Devereux, C. M. Rudin, et al. 2009. A primary xenograft model of small-cell lung cancer reveals irreversible changes in gene expression imposed by culture in vitro. Cancer Res. 69:3364–3373.
26. Tiberio, C., P. Barba, M. C. Magli, F. Arvelo, T. Le Chevalier, M. F. Poupon, et al. 1994. *Hox* gene expression in human small-cell lung cancers xenografted into nude mice. Int. J. Cancer 58:608–615.
27. Lechner, J. F., J. M. Fugaro, Y. Wong, H. I. Pass, C. C. Harris, and S. A. Belinsky. 2001. Perspective: cell differentiation theory may advance early detection of and therapy for lung cancer. Radiat. Res. 155:235–238.
28. Cantile, M., R. Franco, A. Tschan, D. Baumhoer, I. Zlobec, G. Schiavo, et al. 2009. *Hox*D13 expression across 79 tumor tissue types. Int. J. Cancer 125:1532–1541.
29. Grier, D. G., A. Thompson, A. Kwasniewska, G. J. McGonigle, H. L. Halliday, and T. R. Lappin. 2005. The pathophysiology of *Hox* genes and their role in cancer. J. Pathol. 205:154–171.
30. Adams, N. C., T. Tomoda, M. Cooper, G. Dietz, and M. E. Hatten. 2002. Mice that lack astrotactin have slowed neuronal migration. Development 129:965–972.
31. Wu, Q., and T. Maniatis. 1999. A striking organization of a large family of human neural cadherin-like cell adhesion genes. Cell 97:779–790.
32. Shi, D., X. M. Qiu, and Y. F. Bao. 2013. Effects of Helicobacter pylori infection on MUC5AC protein expression in gastric cancer. Future Oncol. 9:115–120.
33. Liu, J., G. Li, X. Peng, B. Liu, B. Yin, X. Tan, et al. 2004. The cloning and preliminarily functional analysis of the human neurotrimin gene. Sci. China C Life Sci. 47:158–164.
34. Sun, C. K., K. Man, K. T. Ng, J. W. Ho, Z. X. Lim, Q. Cheng, et al. 2008. Proline-rich tyrosine kinase 2 (Pyk2) promotes proliferation and invasiveness of hepatocellular carcinoma cells through c-Src/ERK activation. Carcinogenesis 29:2096–2105.
35. Behmoaram, E., K. Bijian, S. Jie, Y. Xu, A. Darnel, T. A. Bismar, et al. 2008. Focal adhesion kinase-related proline-rich tyrosine kinase 2 and focal adhesion kinase are co-overexpressed in early-stage and invasive ErbB-2-positive breast cancer and cooperate for breast cancer cell tumorigenesis and invasiveness. Am. J. Pathol. 173:1540–1550.
36. Lim, E., E. Belcher, Y. K. Yap, A. G. Nicholson, and P. Goldstraw. 2008. The role of surgery in the treatment of limited disease small cell lung cancer: time to reevaluate. J. Thorac. Oncol. 3:1267–1271.
37. Schreiber, D., J. Rineer, J. Weedon, D. Vongtama, A. Wortham, A. Kim, et al. 2010. Survival outcomes with use of surgery in limited-stage small cell lung cancer: should its role be re-evaluated? Cancer 116:1350–1357.
38. Inoue, M., N. Sawabata, and M. Okumura. 2012. Surgical intervention for small-cell lung cancer: what is the surgical role? Gen. Thorac. Cardiovasc. Surg. 60:401–405.
39. Ui-Tei, K., Y. Naito, F. Takahashi, T. Haraguchi, H. Ohki-Hamazaki, A. Juni, et al. 2004. Guidelines for the selection of highly effective siRNA sequences for mammalian and chick RNA interference. Nucleic Acids Res. 32:936–948.
40. Ui-Tei, K., Y. Naito, and K. Saigo. 2006. Essential notes regarding the design of functional siRNAs for efficient mammalian RNAi. J. Biomed. Biotechnol. 2006:65052.

Supporting Information

Additional Supporting Information may be found in the online version of this article:

Table S1. Primer sequences of RT-PCR for *HOTAIR* quantification as well as *GAPDH* and *ACTB* as controls. Also, primers for RNAi experiments are shown.
Table S2. Univariate and multivariate analysis of DSS and RFS/DFS.
Table S3. *HOTAIR* expression mainly associated with genes contributes to cell adhesion.

Role of lymphatic invasion in the prognosis of patients with clinical node-negative and pathologic node-positive lung adenocarcinoma

Takahiro Mimae, MD, PhD,[a] Yasuhiro Tsutani, MD, PhD,[a] Yoshihiro Miyata, MD, PhD,[a] Tomoharu Yoshiya, MD,[a] Yuta Ibuki, MD,[a] Kei Kushitani, MD, PhD,[b] Yukio Takeshima, MD, PhD,[b] Haruhiko Nakayama, MD, PhD,[c] Sakae Okumura, MD, PhD,[d] Masahiro Yoshimura, MD, PhD,[e] and Morihito Okada, MD, PhD[a]

Objective: Some patients with clinical T1 N0 M0 lung adenocarcinoma have pathologic lymph node metastasis. However, neither the precise prognosis nor the factors predictive of the prognosis of such patients have yet been identified.

Methods: Our study included 609 patients with clinical T1 N0 M0 lung adenocarcinoma; 568 (93.3%) pathologic node negative [pN(–)] and 41 (6.7%) pathologic node positive [pN(+)] patients, diagnosed after complete surgical resection. The association between prognosis and pathologic findings was analyzed retrospectively.

Results: pN(+) patients had a significantly lower lepidic growth component ratio (10% vs 50%), a higher lymphatic invasion (LI) rate (68% vs 11%), vessel invasion rate (59% vs 14%), and visceral pleural invasion rate (29% vs 9%), compared with pN(–) patients (all *P*s < .001). Surprisingly, 13 of 41 (32%) pN(+) patients showed no LI. In pN(–) patients, a multivariate analysis of recurrence-free survival revealed that lower lepidic growth component ratio, and lymphatic, vessel, and pleural invasion were significantly correlated with a poor prognosis ($P = .008$, .045, .031, and .024). However, in pN(+) patients, the multivariate analysis of recurrence-free survival showed that only LI was a significant independent prognostic factor ($P = .037$). The 5-year recurrence-free survival rates were as follows: 91.2% for pN(–)/LI(–) patients, 68.2% for pN(–)/LI(+) patients, 63.5% for pN(+)/LI(–) patients, and 41.9% for pN(+)/LI(+) patients. LI status stratified the prognosis not only in patients with no nodal metastasis but also in those with metastasis.

Conclusions: LI, which is not always present in node-positive adenocarcinoma, is an important prognostic variable in patients with node involvement. (J Thorac Cardiovasc Surg 2014;147:1820-6)

Fluorescence deoxyglucose (FDG) positron emission tomography (PET) is commonly used for preoperative assessment of primary tumors, lymph nodes, and distant metastasis to determine staging and treatment strategy,[1-3] thereby improving the accuracy of the definition of clinical stage IA compared with only computed tomography assessment.[1] This has changed the population of patients with clinical stage IA lung adenocarcinoma.[1,4-7] However, some clinical lymph node-negative [cN(–)] patients show positive pathologic lymph node [pN(+)] metastasis. It is speculated that a cN(–) but pN(+) status indicates an initial lymph node metastatic condition, because the accumulation of FDG in the lymph node could be significantly higher in patients with massive lymph node metastasis. Therefore, cN(–)/pN(+) patients may have a better prognosis than cN(+)/pN(+) patients, or a similar prognosis to cN(–)/pN(–) patients. In addition, no studies have identified the prognostic factors in cN(–)/pN(+) patients.

In our study, we evaluated the clinicopathologic findings and prognosis of patients with clinical T1 N0 M0 lung adenocarcinoma according to lymph node status, or other pathologic status. First, we examined the pathologic findings to identify predictive factors for recurrence-free survival (RFS) among patients with clinical stage IA lung adenocarcinoma. Multivariate analysis revealed that lymphatic invasion (LI) status was a predictive factor, both in patients with and without node involvement. Next, we assessed the prognosis of patients with and without lymph node involvement according to LI status. The results highlight the importance of the LI status in patients with clinical T1 N0 M0 lung adenocarcinoma.

MATERIALS AND METHODS

Patient Population

Our study included 611 patients who underwent complete surgical resection of clinical stage IA lung adenocarcinoma at the Hiroshima University

From the Departments of Surgical Oncology[a] and Pathology,[b] Hiroshima University, Hiroshima, Japan; Department of Thoracic Surgery,[c] Kanagawa Cancer Center, Yokohama, Japan; Department of Thoracic Surgery,[d] Cancer Institute Hospital, Tokyo, Japan; and Department of Thoracic Surgery,[e] Hyogo Cancer Center, Akashi, Japan.

Disclosures: Authors have nothing to disclose with regard to commercial support.
Received for publication Aug 5, 2013; revisions received Oct 22, 2013; accepted for publication Nov 22, 2013; available ahead of print Feb 7, 2014.

Address for reprints: Morihito Okada, MD, PhD, Department of Surgical Oncology, Hiroshima University, Hiroshima, Japan, 1-2-3 Kasumi, Minami-ku, Hiroshima, 734-8551, Japan (E-mail: morihito1217@hiroshima-u.ac.jp).

0022-5223/$36.00

http://dx.doi.org/10.1016/j.jtcvs.2013.11.050

Abbreviations and Acronyms
CT = computed tomography
FDG = fluorescence deoxyglucose
GGO = ground glass opacity
HU = Haunsfield unit
LC = lepidic component
LI = lymphatic invasion
OS = overall survival
PET = positron emission tomography
RFS = recurrence-free survival
SUV = standardized uptake value

Hospital (Hiroshima, Japan), the Kanagawa Cancer Centre (Yokohama, Japan), the Cancer Institute Hospital (Tokyo, Japan), and the Hyogo Cancer Centre (Akashi, Japan) between April 2007 and December 2010. Approval was given by the institutional review boards of the participating institutions, all of which waived the requirement for informed consent from individual patients for this retrospective review of the prospective database. Two patients were excluded because they lacked a lepidic component (LC) ratio. The data from the remaining 609 patients were analyzed retrospectively. High-resolution computed tomography (CT) and FDG-PET/CT, followed by a curative R0 resection were performed for all patients staged according to the TNM Classification of Malignant Tumours.[8] Endobronchial ultrasonography or mediastinoscopy was not performed routinely because all patients underwent preoperative high-resolution CT and FDG-PET/CT; the high-resolution CT results showed no swelling of mediastinal or hilar lymph nodes and FDG-PET revealed no accumulation of FDG in those lymph nodes. Lymph node swelling was defined when the diameter of a minor axis is larger than 10 mm. Sublobar resection was performed in cases of complete removal of the disease with appropriate surgical margins for a peripheral T1a N0 M0 tumor. Wedge resection without lymph node assessment was performed for ground glass opacity (GGO) tumors on high-resolution CT, which was regarded as a node-negative and noninvasive tumor in a prospective study.[9] Segmentectomy with hilar and mediastinal lymph node dissection were performed for a GGO-mixed tumor. If lymph node involvement was detected on an intraoperative frozen section of any lymph node, the procedure was converted to a standard lobectomy. All other patients underwent a standard lobectomy. The inclusion criteria included preoperative staging determined by high-resolution CT and FDG-PET/CT, curative surgery without any induction therapy, and a definitive histopathologic diagnosis of lung adenocarcinoma. Patients with incompletely resected tumors (R1 or R2), and those with multiple tumors or previous lung surgery, were excluded from the data set.

Pathology Studies

Sections were fixed with 10% formalin and embedded in paraffin. Consecutive 4-μm sections were cut and 1 slice per 5 mm was examined under a microscope for the pathologic assessment. Histologic diagnosis and staging was based on the latest edition of the World Health Organization classification scheme.[10] The histologic type of adenocarcinoma and the presence of lymphatic involvement were determined using hematoxylin-eosin stained tissue. If the findings could not be determined by hematoxylin-eosin staining alone, immunohistochemical staining was carried out as necessary. An LC ratio was defined as the proportion of LC area relative to the entire tumor. LI and blood vessel invasion were assessed by immunohistochemistry for D2-40, which stains lymphatic ducts, and Van Gieson staining of the elastic fiber of the vessels. LI and blood vessel invasion were determined when spreading through or penetration was detected as an extension of a malignant neoplasm. To evaluate pleural invasion, elastic tissue fibers were subjected to Van Gieson staining. Pleural invasion was determined if cancer cells had invaded beyond the elastic layer, including invasion into the visceral pleural surface, or neighboring organs. Histologic examinations were determined by pathologists from each institution for the purposes of this study.

HRCT

A 16-row multidetector CT was used to obtain chest images. For high-resolution images of the tumors, the following parameters were used: 120 kVp, 200 mA, 1 to 2 mm section thickness, 512 × 512 pixel resolution, 0.5 to 1.0 second scanning time, a high spatial reconstruction algorithm with a 20 cm field of view, and mediastinal (level, 40 Haunsfield unit [HU]; width, 400 HU) and lung (level, −600 HU; width, 1600 HU) window settings. GGO was defined as a misty increase in lung attenuation that did not obscure underlying vascular markings. CT scans were reviewed and tumor sizes determined by radiologists from each institution.

FDG-PET/CT

Patients were instructed to fast for at least 4 hours before intravenous injection of 74 to 370 MBq FDG and then to relax for at least 1 hour before the FDG-PET/CT scan. For imaging, Biograph Sensation 16 (Siemens Healthcare, Erlangen, Germany), Aquiduo (Toshiba Medical Systems Corporation, Tochigi, Japan), or Discovery ST (GE Healthcare, Little Chalfont, United Kingdom) integrated 3-dimensional PET/CT scanners were used. Low-dose nonenhanced CT images of 2 to 4 mm section thickness were taken from the head to the pelvis of each patient. An anthropomorphic body phantom (NEMA NU2-2001; Data Spectrum Corp, Hillsborough, NC) was used to minimize variations in standardized uptake values (SUVs) among the institutions.[11,12] The original SUV_{max} values were determined by radiologists from each institution for the purposes of this study. On FDG-PET/CT images, all lymph nodes in the thorax with FDG uptake no greater than the normal background activity of the mediastinal blood pool—the SUV_{max} of which was <1.5, regardless of size—were considered cN0. A lymph node where the SUV_{max} was ≥1.5 or more was considered "suspicious for malignancy." However, even lymph nodes with high FDG uptake, when they showed higher attenuation than mediastinal structures (great vessels) or benign calcification (central, nodular, diffuse, or popcorn-like), were also considered benign.[13]

Follow-up Evaluation

All patients who underwent lung resections were followed-up from the day after surgery. Postoperative follow-up procedures, including a physical examination and chest radiograph every 3 months and chest and abdominal CT examinations every 6 months, were performed for the first 2 years. Thereafter, a physical examination and chest radiograph were performed every 6 months, and a chest CT examination was performed annually.

Statistical Analyses

Patients with clinical stage IA lung adenocarcinoma were included in the analysis. A Mann-Whitney *U* test was used to compare continuous variables and the χ^2 test or Fisher exact test was used for categorical variables. RFS was defined as the length of time after primary surgical treatment for a cancer ends that the patient survived without any sign or symptom of the cancer. Recurrence was defined as patients having symptoms caused by recurring cancer and suspicious lesions that were diagnosed as recurrent tumors by biopsies. If suspicious lesions were not diagnosed as recurrence, by biopsy, the "recurrence" was comprehensively and clinically defined by radiographic findings, including CT and FDG-PET/CT. RFS and overall survival (OS) curves were calculated using the Kaplan-Meier method. Univariate survival analysis was performed using the log-rank test for comparisons of curves. A Cox regression model was used to calculate *P* values and hazard ratios in the univariate and multivariate analyses. The prognostic analysis was performed during August 2012. All statistical analyses were

GTS

performed using EZR (Saitama Medical Centre, Jichi Medical University, Saitama, Japan),[14] which is a graphical user interface for R (The R Foundation for Statistical Computing, version 2.13.0, Vienna, Austria). More precisely, it is a modified version of R Commander (version 1.6-3), which includes statistical functions frequently used in biostatistics.

RESULTS

Clinical Outcomes in Patients With Lung Adenocarcinoma

The median follow-up time was 41.6 months. Lobectomy, segmentectomy, and wedge resection were performed in 375, 97, and 137 patients, respectively. The 30-day mortality rate was 0%. As shown in Table 1, 41 patients (6.7%) had lymph node metastasis in the clinical stage IA lung adenocarcinoma cohort. No significant difference between pN(–) and pN(+) patients was detected in terms of age, sex, and carcinoembryonic antigen value, whereas a marginal difference was seen for tumor size on preoperative high-resolution CT. Regarding the clinical variables, lower GGO ratios and higher SUV_{max} were observed in the N+ group compared with the N– group. In terms of pathologic variables, a lower LC ratio and higher positive rate of LI, blood vessel invasion, and pleural invasion were detected in pN(+) patients. Thirteen of 41 pN(+) patients showed no LI. As shown in Figure 1, *A*, clinical stage IA lung adenocarcinoma patients with lymph node metastasis had a lower RFS rate than those without lymph node metastasis ($P < .001$).

Univariate and Multivariate Analyses of Prognosis According to Pathologic Variables, by Lymph Node Status

Univariate and multivariate analyses of the clinical and pathologic variables were performed to ascertain the most important predictive factor. Univariate analyses were performed on RFS and OS, whereas further analyses, including multivariate analyses, were performed on RFS because OS was more immature than RFS. The pathologic variables included LC ratio, LI status, blood vessel invasion status, pleural invasion status, and lymph node status. For the LC ratio, 30% was used as a threshold because this is the borderline for cT1 N0 M0 lung adenocarcinoma classified as a high- or low-grade malignancy.[2] Univariate analysis revealed that pN(+) patients with LI positive status [LI(+)] had a marginally poorer prognosis ($P = .059$), whereas a lower LC ratio and LI+ status, blood vessel invasion, pleural invasion, or lymph node metastasis was significantly correlated with a poor prognosis in both all patients in this cohort, and in pN(–) patients (Table 2). Additionally, multivariate analysis showed that only LI positive status was a prognostic factor in pN(+) patients ($P = .037$), whereas a lower LC ratio and positive LI status, blood vessel invasion, pleural invasion, or lymph node metastasis were prognostic factors in both all patients and pN(–) patients (Table 3).

TABLE 1. Clinicopathologic findings in patients with clinical stage IA lung adenocarcinoma with or without lymph node metastasis

Finding	Node negative (n = 568)	Node positive (n = 41)	*P* value
Age			
Median	66	65	.33
Interquartile range	60.75-73	56-73	
Sex			
Female	322 (57%)	22 (54%)	.19
Male	246 (43%)	19 (46%)	
CEA			
Median	2.5	3.6	.25
Interquartile range	1.5-3.6	1.1-113.8	
Size*			
Median	2.0	2.2	.060
Interquartile range	1.5-2.4	2.55-4.2	
GGO† ratio			
Median	40	0	<.001
Interquartile range	10-80	0-10	
SUV max			
Median	1.5	3.6	<.001
Interquartile range	0.9-2.6	2.3-4.9	
LC ratio			
Median	50	10	<.001
Interquartile range	10-90	0-20	
Lymphatic invasion			
Negative	507 (89%)	13 (32%)	<.001
Positive	61 (11%)	28 (68%)	
Blood vessel invasion			
Negative	488 (86%)	17 (41%)	<.001
Positive	80 (14%)	24 (59%)	
Pleural invasion			
Negative	515 (91%)	29 (71%)	<.001
Positive	53 (9%)	12 (29%)	

CEA, Carcinoembryonic antigen; *GGO*, ground-glass opacity; *SUV*, standardized uptake value; *LC*, lepidic component. *Tumor size on the high-resolution computed tomography scan. †GGO ratio on the high-resolution computed tomography scan.

Next, we assessed the RFS of pN(–) and pN(+) patients according to their LI status. In both pN(–) and pN(+) patients, RFS rates were lower in LI(+) status compared with LI negative status [LI(–)] ($P < .001$ and $P = .059$) (Figure 1, *B* and *C*). The 3-year RFS and OS rates for each group was as follows: pN(–)/LI(–) 93.4% and 96.7%, pN(–)/LI(+) 70.8% and 85.1%, pN(+)/LI(–) 84.6% and 92.3%, and pN(+)/LI(+) 47.9% and 75.0%, respectively (Table 2 and Figure 1, *B-F*). No significant difference was detected between the pN(+)/LI(–) and pN(–)/LI(+) patients for RFS ($P = .62$; Figure 1, *D*), whereas pN(+)/LI(–) and pN(–)/LI(–) patients, pN(+)/LI(+) and pN(–)/LI(–) patients, and pN(+)/LI(+) and pN(–)/LI(+) patients exhibited significantly different RFS values ($P = .022$, <.001, and .011, respectively).

Clinicopathologic Findings in N+ Patients

In N+ patients, there were no significant differences between the LI(–) and LI(+) groups in terms of age, sex,

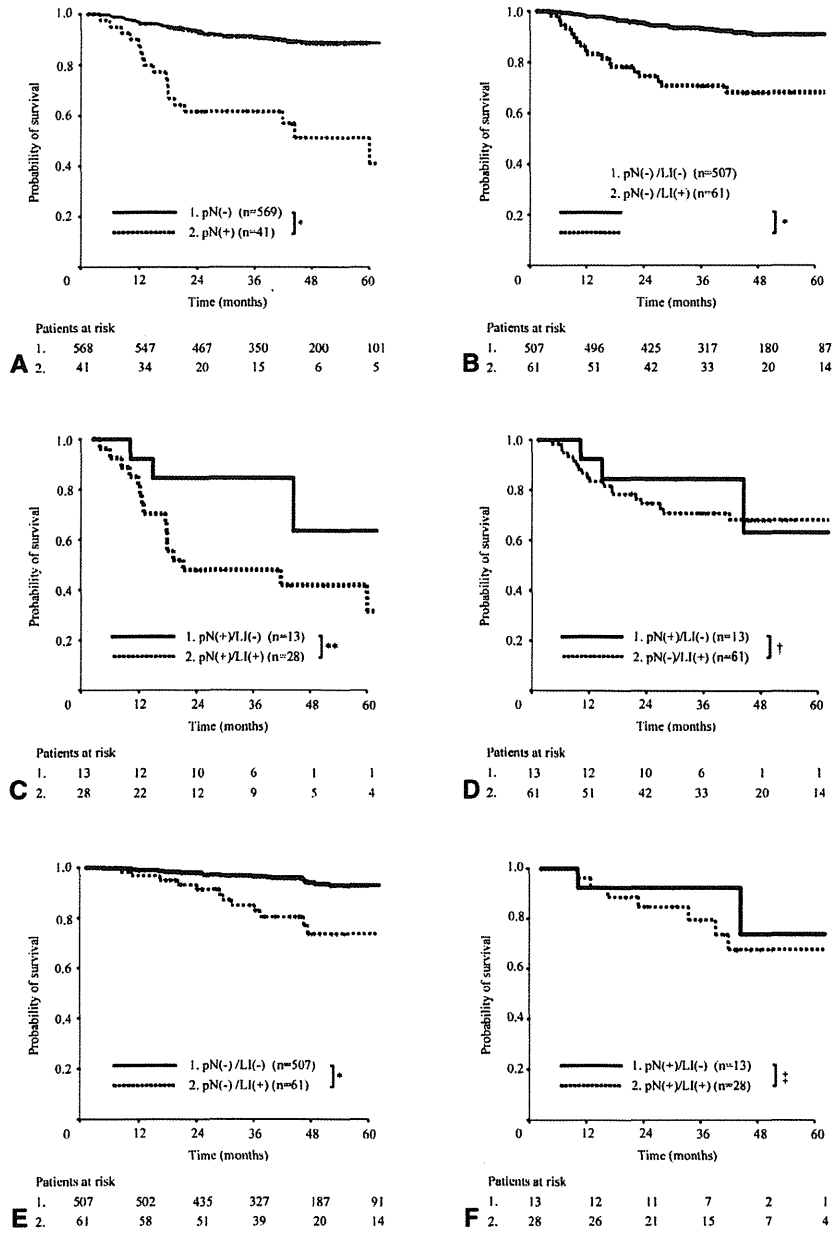

FIGURE 1. Kaplan-Meier recurrence-free survival (A-D) and overall survival (E and F) curves in patients with clinical stage IA lung adenocarcinoma according to pathologic lymph node status and lymph node metastasis and lymphatic invasion (*LI*) status. A, Patients are classified into pathologic lymph node metastasis negative (pN[–]) and positive (pN[+]) groups. B, The pN(–) patients are classified into a lymphatic permeation negative (pN[–]/LI[–]) group and a lymphatic permeation positive (pN[–]LI[+]) group. C, The pN(+) patients are classified into a lymphatic permeation negative (N[+]LI[–]) group and a lymphatic permeation positive (N[+]LI[+]) group. D, Recurrence-free survival curves of pN(+)LI(–) and pN(–)LI(+) patients are shown. E, The pN(–) patients are classified into a pN(–)/LI(–) group and a pN(–)LI(+) group. F, The pN(+) patients are classified into an N(+)LI(–) group and an N(+)LI(+) group. *$P < .001$; **$P = .059$; †$P = .62$; ‡$P = .48$.

carcinoembryonic antigen values, preoperative tumor size, and SUV_{max} values. Regarding pathologic findings, LI status had no association with the LC ratio, blood vessel invasion, and pleural invasion. Additionally, LI status had no correlation with lymph node metastasis status, both single or multiple station metastases (Table 4).

DISCUSSION

In this study, pN(+)/LI(–) patients had a better prognosis than pN(+)/LI(+) patients, whereas there were no significant differences in the RFS between pN(+)/LI(–) and pN(–)/LI(+) clinical stage IA lung adenocarcinoma patients at the participating institutions. LI status, which is

TABLE 2. Univariate log-rank analysis of recurrence-free survival (RFS) and overall survival (OS) according to various factors in patients with lung adenocarcinoma

	All		Node negative		Node positive	
Pathologic variable	**3-y RFS rate (%)**	***P* value**	**3-y RFS rate (%)**	***P* value**	**3-y RFS rate (%)**	***P* value**
LC ratio						
≥30	95.2	<.0001	95.9	<.0001	57.1	.93
<30	78.2		81.4		60.5	
Lymphatic invasion						
Negative	93.1	<.0001	93.4	<.0001	84.6	.059
Positive	63.7		70.8		47.9	
Blood vessel invasion						
Negative	93.1	<.0001	94.3	<.0001	58.8	.93
Positive	63.7		71.0		60.6	
Pleural invasion						
Negative	93.1	<.0001	92.6	<.0001	57.1	.42
Positive	68.6		74.6		65.6	
Lymph node metastasis						
Negative	90.9	<.0001	90.9	—	—	—
Positive	59.9		—		59.9	
	All		**Node negative**		**Node positive**	
	3-y OS rate (%)	***P* value**	**3-y OS rate (%)**	***P* value**	**3-y OS rate (%)**	***P* value**
LC ratio						
≥30	97.0	<.0001	97.3	<.0001	75.0	.76
<30	90.9		92.0		84.5	
Lymphatic invasion						
Negative	96.6	<.0001	96.7	<.0001	92.3	.490
Positive	83.5		85.1		75.0	
Blood vessel invasion						
Negative	96.4	<.0001	96.7	<.0001	88.2	.55
Positive	86.5		88.1		81.0	
Pleural invasion						
Negative	94.9	.0042	95.9	<.0001	100.0	.29
Positive	92.7		91.2		77.3	
Lymph node metastasis						
Negative	95.5	<.0001	95.5	—	—	—
Positive	83.6		—		83.6	

LC, Lepidic component; *RFS*, recurrence-free survival; *OS*, overall survival.

not always positive in N+ patients, is a significant predictive factor in patients with pathologic lymph node metastasis, whereas the lymph node metastasis status is a strong prognostic factor in patients with clinical T1 N0 M0 lung adenocarcinoma.

It is reasonable that lymph node metastasis occurs after cancer cells invade the lymphatic vessels around the tumors; however, 13 of 41 (31.7%) patients with lung adenocarcinoma, whose LI status was negative, exhibited metastasis to regional lymph nodes. One possible explanation is the difficulty in examining all slices of a specimen; some of the slices, including the tumor, could be pathologically assessed. This could be missed if tumors had only slight LI, and the LI status would be determined as negative. Therefore, "no pathologic LI" could either mean no massive LI, just a slight invasion, or it could mean that there was indeed no LI. This is especially the case in pN+ patients, where "no pathologic LI" indicates a slight LI. Slight invasion means the initial period of lymphatic vessel invasion and lymph node metastasis; therefore, patients with slight invasion had a better prognosis than those with massive invasion after complete surgical resection. In pN+ patients the N1 rate was higher in pN(+)/LI(–) patients compared with pN(+)/LI(+) patients, albeit nonsignificantly so. This suggests that pN(+)/LI(–) is indicative of initial lymph node metastasis, as described above.

In pN+ patients, the N2:N1 ratio was higher in pN(+) LI(+) than pN(+)LI(–) patients, although the difference was not statistically significant. The number of pN+ patients was too small to draw any conclusion; however, the tumors that showed massive LI had a higher tendency to progress to N2 disease than LI(–) tumors. Patients with

TABLE 3. Multivariate Cox regression analysis of recurrence-free survival according to various factors

	All		Node negative		Node positive	
Pathologic variables	**HR**	***P* value**	**HR**	***P* value**	**HR**	***P* value**
LC ratio	0.44	.010	0.39	.008	1.7	.62
>30 vs <30	0.23-0.82		0.20-0.78		0.44-6.3	
Lymphatic invasion	2.5	.001	1.9	.045	6.1	.037
Positive vs negative	1.4-4.3		1.0-3.5		1.3-28.7	
Blood vessel invasion	1.8	.037	2.0	.031	0.87	.61
Positive vs negative	1.0-3.1		1.1-3.8		0.31-2.4	
Pleural invasion	1.6	.11	2.1	.024	0.47	.19
Positive vs negative	0.91-2.7		1.1-3.9		0.14-1.5	
Lymph node metastasis	1.9	.032	—*	—*	—*	—*
Positive vs negative	1.1-3.4					

LC, Lepidic component; *HR*, hazard ratio. *Not calculated.

GTS

micrometastatic disease to the lymph nodes have been demonstrated to have a worse prognosis than patients with lymph nodes completely replaced by tumors.[15] This suggests that the continuum from LI to lymph node micrometastasis to lymph node replacement might be more complex than previously believed.

As in previous reports, in all patients, multivariate analysis of RFS revealed a lower LC ratio, positive status of lymph nodes, LI, blood vessel invasion, pleural invasion and were poor prognostic factors as well as N+ status in this study.[16,17] In contrast, all evaluated pathologic variables, except for LI status, did not show potential as predictive factors for patients with lymph node involvement. Although lymphatic metastasis status was a strong prognostic factor, LI status was also a significant predictive factor of prognosis in patients with clinical stage IA lung adenocarcinoma. In pN+ patients, LI status had no association with either the clinical or pathologic findings. Thus, the above findings strongly support the significance of LI status as a predictive factor, particularly in patients whose lymph node status is clinically negative and pathologically positive. That is, poor prognosis should be defined according to not only lymph node status but also LI status. Other unknown factors may more precisely determine the true patient population with a poor prognosis. Although pN+ patients typically receive adjuvant chemotherapy, such patients may be classified into no-adjuvant, mild-adjuvant, and severe-adjuvant groups using several predictive factors, including LI status.

Two previous reports have demonstrated that LI status is a poor prognostic factor in surgically resected non–small cell lung cancer[18,19] and a similar result was shown in pathologic stage I or adenocarcinoma patients. Additionally, LI status has been demonstrated to be a prognostic factor regardless of lymph node status.[18,19] However, these previous studies had some limitations; 1 was the quality of LI status evaluation. LI status was evaluated using D2-40 immunostaining in this study, whereas only some tumors were assessed for LI status using D2-40 in the report[19] and the other did not distinguish LI from blood vessel invasion.[18] Thus, the quality of LI evaluation was higher in our study. Another limitation is heterogeneity of the cohort. The analysis was performed only in pathologic stage I patients in the previous studies to minimize heterogeneity.[18,19] However, that analysis of pathologic stage I patients could not assess LI status in pN+ patients. In our study, we evaluated LI status with little heterogeneity in pN+ patients because we included only clinical stage IA adenocarcinoma patients having little heterogeneity.

The rate of lymph node involvement was 6.7% of clinical stage IA lung adenocarcinoma patients in our study (41 out of 609 cases). PET/CT examination has been shown to provide the most accurate preoperative diagnosis[1,4] and results in appropriate treatment. However, a new diagnostic method is necessary to evaluate more accurately the preoperative status of patients with clinical stage IA adenocarcinoma and pathologic lymph node involvement whose preoperative diagnostic modality included a PET scan.

Few patients had lymph node metastasis in clinical stage IA lung adenocarcinoma, which represents one of the main limitations of this study; only a very small number of patients with lymph node involvement had a negative LI status. This makes it difficult to conclude that the prognosis of pN(+)LI(–) patients is equivalent to that of pN(–) LI(+) patients; however, it cannot be denied that LI status plays an important role in assessing patients with lymph node metastasis. The lack of data about pathologic tumor size or morbidity are also limitations of our study. Another is that detailed numbers on patients who received postoperative chemotherapy were not available. Postoperative chemotherapy was performed when pathologic upstaging or recurrence was detected. Additionally, although the follow-up time was too short to assess OS in this study, the OS curves showed similar tendencies to RFS. Because a previous study reported that RFS could be a surrogate

TABLE 4. Clinicopathologic findings in patients with clinical stage IA but pathologic lymph node positive lung adenocarcinoma, according to lymphatic invasion status

Finding	Lymph node metastasis positive: Lymphatic invasion negative (n = 13)	Lymph node metastasis positive: Lymphatic invasion positive (n = 28)	*P* value
Age			
Median	64	66	.96
Interquartile range	56-72	55.25-73.25	
Sex			
Female	4	15	.20
Male	9	13	
CEA			
Median	3.7	3.4	.81
Interquartile range	2.5-4.075	2.65-4.25	
Size*			
Median	2	2.2	.62
Interquartile range	1.6-2.6	1.775-2.5	
GGO† ratio			
Median	0	0	.75
Interquartile range	0-10	0-2.5	
SUV max			
Median	3.4	3.7	.87
Interquartile range	2.7-4.0	2.175-4.925	
LC ratio			
Median	10	10	.16
Interquartile range	10-20	0-12.5	
Blood vessel invasion			
Negative	7	10	.32
Positive	6	18	
Pleural invasion			
Negative	11	18	.28
Positive	2	10	
Lymph node metastasis			
N1	9	11	.18
Single station N2 or single station N2 + N1	2	11	
Multistation N2	2	6	

CEA, Carcinoembryonic antigen; *GGO*, ground-glass opacity; *SUV*, standardized uptake value; *LC*, lepidic component. *Tumor size on the high-resolution computed tomography scan. †GGO ratio on the high-resolution computed tomography scan.

for OS,[20] to evaluate RFS may effectively be equivalent to assessing OS in identifying prognostic factors.

CONCLUSIONS

LI was not always present in pN+ adenocarcinoma patients. In addition, pN(+)LI(−) patients had a better prognosis than pN(+)LI(+) patients, whereas there was no significant difference in RFS between pN(+)LI(−) and pN(−)LI(+) patients with clinical stage IA lung adenocarcinoma. LI status was indicated to classify clinical T1 N0 M0 lung adenocarcinoma patients with and without lymph node involvement into good and poor prognosis groups, the preoperative staging of which conducted using high-resolution CT and FDG-PET/CT. LI status may affect the selection of patients who have to receive adjuvant therapy.

References

1. Lardinois D, Weder W, Hany TF, Kamel EM, Korom S, Seifert B, et al. Staging of non-small-cell lung cancer with integrated positron-emission tomography and computed tomography. *N Engl J Med*. 2003;348:2500-7.
2. Okada M, Nakayama H, Okumura S, Daisaki H, Adachi S, Yoshimura M, et al. Multicenter analysis of high-resolution computed tomography and positron emission tomography/computed tomography findings to choose therapeutic strategies for clinical stage IA lung adenocarcinoma. *J Thorac Cardiovasc Surg*. 2011;141:1384-91.
3. Tsutani Y, Miyata Y, Nakayama H, Okumura S, Adachi S, Yoshimura M, et al. Prediction of pathologic node-negative clinical stage IA lung adenocarcinoma for optimal candidates undergoing sublobar resection. *J Thorac Cardiovasc Surg*. 2012;144:1365-71.
4. Shim SS, Lee KS, Kim BT, Chung MJ, Lee EJ, Han J, et al. Non-small cell lung cancer: prospective comparison of integrated FDG PET/CT and CT alone for preoperative staging. *Radiology*. 2005;236:1011-9.
5. Kim BT, Lee KS, Shim SS, Choi JY, Kwon OJ, Kim H, et al. Stage T1 non-small cell lung cancer: preoperative mediastinal nodal staging with integrated FDG PET/CT—a prospective study. *Radiology*. 2006;241:501-9.
6. Yi CA, Lee KS, Kim BT, Shim SS, Chung MJ, Sung YM, et al. Efficacy of helical dynamic CT versus integrated PET/CT for detection of mediastinal nodal metastasis in non-small cell lung cancer. *AJR Am J Roentgenol*. 2007;188:318-25.
7. Lee SM, Park CM, Paeng JC, Im HJ, Goo JM, Lee HJ, et al. Accuracy and predictive features of FDG-PET/CT and CT for diagnosis of lymph node metastasis of T1 non-small-cell lung cancer manifesting as a subsolid nodule. *Eur Radiol*. 2012;22:1556-63.
8. Goldstraw P, Crowley J, Chansky K, Giroux DJ, Groome PA, Rami-Porta R, et al. The IASLC Lung Cancer Staging Project: proposals for the revision of the TNM stage groupings in the forthcoming (seventh) edition of the TNM Classification of malignant tumours. *J Thorac Oncol*. 2007;2:706-14.
9. Suzuki K, Koike T, Asakawa T, Kusumoto M, Asamura H, Nagai K, et al. A prospective radiological study of thin-section computed tomography to predict pathological noninvasiveness in peripheral clinical IA lung cancer (Japan Clinical Oncology Group 0201). *J Thorac Oncol*. 2011;6:751-6.
10. Travis WD, Brambilla E, Muller-Hermelink HK, Harris CC. Pathology and genetics tumors of the lung, pleura, thymus and heart. In: World Health Organization classification of tumours. Lyon, France: IARC Press; 2004.
11. Nakayama H, Okumura S, Daisaki H, Kato Y, Uehara H, Adachi S, et al. Value of integrated positron emission tomography revised using a phantom study to evaluate malignancy grade of lung adenocarcinoma: a multicenter study. *Cancer*. 2010;116:3170-7.
12. Delbeke D, Coleman RE, Guiberteau MJ, Brown ML, Royal HD, Siegel BA, et al. Procedure guideline for tumor imaging with 18F-FDG PET/CT 1.0. *J Nucl Med*. 2006;47:885-95.
13. Li L, Ren S, Zhang Y, Guan Y, Zhao J, Liu J, et al. Risk factors for predicting the occult nodal metastasis in T1-2N0M0 NSCLC patients staged by PET/CT: potential value in the clinic. *Lung Cancer*. 2013;81:213-7.
14. Kanda Y. Investigation of the freely available easy-to-use software 'EZR' for medical statistics. *Bone Marrow Transplant*. 2013;48:452-8.
15. Riquet M, Bagan P, Le Pimpec Barthes F, Banu E, Scotte F, Foucault C, et al. Completely resected non-small cell lung cancer: reconsidering prognostic value and significance of N2 metastases. *Ann Thorac Surg*. 2007;84:1818-24.
16. Funai K, Sugimura H, Morita T, Shundo Y, Shimizu K, Shiiya N. Lymphatic vessel invasion is a significant prognostic indicator in stage IA lung adenocarcinoma. *Ann Surg Oncol*. 2011;18:2968-72.
17. Kudo Y, Saji H, Shimada Y, Nomura M, Matsubayashi J, Nagao T, et al. Impact of visceral pleural invasion on the survival of patients with non-small cell lung cancer. *Lung Cancer*. 2012;78:153-60.
18. Higgins KA, Chino JP, Ready N, D'Amico TA, Berry MF, Sporn T, et al. Lymphovascular invasion in non-small-cell lung cancer: implications for staging and adjuvant therapy. *J Thorac Oncol*. 2012;7:1141-7.
19. Wang J, Wang B, Zhao W, Guo Y, Chen H, Chu H, et al. Clinical significance and role of lymphatic vessel invasion as a major prognostic implication in non-small cell lung cancer: a meta-analysis. *PloS One*. 2012;7:e52704.
20. Gill S, Sargent D. End points for adjuvant therapy trials: has the time come to accept disease-free survival as a surrogate end point for overall survival? *Oncologist*. 2006;11:624-9.

Published OnlineFirst April 11, 2014; DOI: 10.1158/1078-0432.CCR-14-0107

Clinical Cancer Research

Human Cancer Biology

Druggable Oncogene Fusions in Invasive Mucinous Lung Adenocarcinoma

Takashi Nakaoku[1,8], Koji Tsuta[4], Hitoshi Ichikawa[2], Kouya Shiraishi[1], Hiromi Sakamoto[2], Masato Enari[3], Koh Furuta[4], Yoko Shimada[1], Hideaki Ogiwara[1], Shun-ichi Watanabe[5], Hiroshi Nokihara[6], Kazuki Yasuda[7], Masaki Hiramoto[7], Takao Nammo[7], Teruhide Ishigame[9], Aaron J. Schetter[9], Hirokazu Okayama[9], Curtis C. Harris[9], Young Hak Kim[8], Michiaki Mishima[8], Jun Yokota[1,10], Teruhiko Yoshida[2], and Takashi Kohno[1]

Abstract

Purpose: To identify druggable oncogenic fusions in invasive mucinous adenocarcinoma (IMA) of the lung, a malignant type of lung adenocarcinoma in which *KRAS* mutations frequently occur.

Experimental Design: From an IMA cohort of 90 cases, consisting of 56 cases (62%) with *KRAS* mutations and 34 cases without (38%), we conducted whole-transcriptome sequencing of 32 IMAs, including 27 cases without *KRAS* mutations. We used the sequencing data to identify gene fusions, and then performed functional analyses of the fusion gene products.

Results: We identified oncogenic fusions that occurred mutually exclusively with *KRAS* mutations: *CD74-NRG1*, *SLC3A2-NRG1*, *EZR-ERBB4*, *TRIM24-BRAF*, and *KIAA1468-RET*. *NRG1* fusions were present in 17.6% (6/34) of *KRAS*-negative IMAs. The *CD74-NRG1* fusion activated HER2:HER3 signaling, whereas the *EZR-ERBB4* and *TRIM24-BRAF* fusions constitutively activated the ERBB4 and BRAF kinases, respectively. Signaling pathway activation and fusion-induced anchorage-independent growth/tumorigenicity of NIH3T3 cells expressing these fusions were suppressed by tyrosine kinase inhibitors approved for clinical use.

Conclusions: Oncogenic fusions act as driver mutations in IMAs without *KRAS* mutations, and thus represent promising therapeutic targets for the treatment of such IMAs. *Clin Cancer Res; 20(12); 3087–93. ©2014 AACR.*

Introduction

Oncogene fusions have recently been identified as driver mutations and (possible) therapeutic targets in lung adenocarcinoma (LADC), a major histologic type of lung cancer (1). Such fusions include *EML4-* or *KIF5B-ALK*, *KIF5B*, or *CCDC6-RET*, and *CD74-*, *EZR-*, or *SLC34A2-ROS1* (2–9). These oncogene fusions occur mutually exclusively with one another, and with other targetable oncogene aberrations such as *EGFR*, *KRAS*, *BRAF*, and *HER2* mutations. Therefore, molecular targeted therapy combined with the identification of driver oncogene aberrations represents a powerful and promising approach to personalized treatment of LADC (10, 11).

Invasive mucinous adenocarcinoma (IMA) of the lung is composed predominantly of goblet cells. IMA is morphologically characterized by tall columnar cells with basal nuclei and a pale cytoplasm containing varying amounts of mucin (12, 13). IMAs, which constitute 2% to 10% of all LADCs in Japan, the United States, and European countries (14–16), are indicated as being more malignant than more common types of LADC, such as acinar or papillary adenocarcinoma. The *KRAS* mutation is the only driver aberration commonly detected in IMAs (in 50%–80% of cases). To date, no driver gene aberrations have been detected in *KRAS*-negative IMAs; these aberrations must be identified to facilitate the development of effective treatments for such cancers. Therefore, we performed whole-transcriptome sequencing (RNA sequencing) of IMAs lacking *KRAS* mutations to identify novel chimeric fusion transcripts that represent potential targets for cancer therapy.

Authors' Affiliations: Divisions of [1]Genome Biology, [2]Genetics, and [3]Refractory Cancer Research, National Cancer Center Research Institute, Divisions of [4]Pathology and Clinical Laboratories, [5]Thoracic Surgery, and [6]Thoracic Oncology, National Cancer Center Hospital, Chuo-ku; [7]Department of Metabolic Disorder, Diabetes Research Center, Research Institute, National Center for Global Health and Medicine, Shinjuku-ku, Tokyo; [8]Department of Respiratory Medicine, Graduate School of Medicine, Kyoto University, Yoshida-Konoe-cho, Sakyo-ku, Kyoto, Japan; [9]Laboratory of Human Carcinogenesis, Center for Cancer Research, National Cancer Institute, NIH, Bethesda, Maryland; and [10]The Institute of Predictive and Personalized Medicine of Cancer (IMPPC), Barcelona, Spain

Note: Supplementary data for this article are available at Clinical Cancer Research Online (http://clincancerres.aacrjournals.org/).

Corresponding Author: Takashi Kohno, Division of Genome Biology, National Cancer Center Research Institute, 5-1-1 Tsukiji, Chuo-ku, Tokyo 104-0045, Japan. Phone: 81-3-3542-2511; Fax: 81-3-3542-0807; E-mail: tkkohno@ncc.go.jp

doi: 10.1158/1078-0432.CCR-14-0107

Published OnlineFirst April 11, 2014; DOI: 10.1158/1078-0432.CCR-14-0107

Translational Relevance

Oncogene fusions, such as the *ALK*, *RET*, and *ROS1* fusions, have recently been revealed as therapeutic targets in lung adenocarcinoma (LDAC). We identified multiple druggable oncogene fusions, including those involving the *NRG1*, *ERBB4*, and *BRAF* genes, in invasive mucinous adenocarcinoma (IMA), a malignant type of LDAC. The fusions occurred mutually exclusively with *KRAS* mutations, a common driver oncogene aberration in IMA. These fusions represent potentially clinically relevant targets for treatment of IMAs that lack *KRAS* mutations.

Materials and Methods

Samples

Ninety IMAs were identified among consecutive patients with primary adenocarcinoma of the lung who were treated surgically at the National Cancer Center Hospital, Tokyo, Japan, from 1998 to 2013. Histologic diagnoses were based on the most recent World Health Organization classification and the International Association for the Study of Lung Cancer/American Thoracic Society/European Respiratory Society (IASLC/ATS/ERS) criteria for LADC (13, 17). Total RNA was extracted from grossly dissected, snap-frozen tissue samples using TRIzol (Invitrogen). The study was approved by the Institutional Review Boards of the participating institutions.

RNA sequencing

RNA sequencing libraries were prepared from 1 or 2 μg of total RNA using the mRNA-Seq Sample Prep Kit or TruSeq RNA Sample Prep Kit (Illumina). The resultant libraries were subjected to paired-end sequencing of 50 or 75 bp reads on a Genome Analyzer IIx (GAIIx) or HiSeq 2000 (Illumina). Fusion transcripts were detected using the TopHat-Fusion algorithm (18). Experimental conditions for RNA sequencing are described in Supplementary Table S1.

Examinations of oncogenic properties of fusion products

To construct lentiviral vectors for expression of the CD74-NRG1, EZR-ERBB4, and TRIM24-BRAF fusion proteins, full-length cDNAs were amplified from tumor cDNA by PCR and inserted into pLenti-6/V5-DEST plasmids (Invitrogen). The integrity of each inserted cDNA was verified by Sanger sequencing. Expression of fusion products of the predicted sizes was confirmed by Western blot analysis of transiently transfected and virally infected cells (Supplementary Fig. S1A). Details of plasmid transfection, viral infection, Western blot analysis, and soft agar colony and tumorigenicity assays are described in Supplementary Materials and Methods.

Results and Discussion

We prepared an IMA cohort of 90 cases consisting of 56 (62%) cases with *KRAS* mutations and 34 (38%) cases without. The 34 *KRAS*-negative cases included two, one, and one cases with *BRAF* mutation, *EGFR* mutation, and *EML4-ALK* fusion, respectively; the remaining 30 were "pan negative" for representative driver aberrations in LADCs. Thirty-two cases, consisting of 27 pan-negative and five *KRAS* mutation-positive cases, were subjected to RNA sequencing (Supplementary Table S1). Analysis of $>2 \times 10^7$ paired-end reads obtained by RNA sequencing and subsequent validation by Sanger sequencing of reverse transcription PCR (RT-PCR) products revealed five novel gene-fusion transcripts detected only in the pan-negative IMAs: *CD74-NRG1*, *SLC3A2-NRG1*, *EZR-ERBB4*, *TRIM24-BRAF*, and *KIAA1468-RET* (Fig. 1A and B; Table 1; details in Supplementary Materials and Methods; Supplementary Fig. S2 and Supplementary Table S2). RT-PCR screening of these fusions in the remaining 58 IMAs that had not been subjected to RNA sequencing revealed one additional pan-negative case with the *CD74-NRG1* fusion. Thus, the *CD74-NRG1* fusion, detected in five of 34 (14.7%) cases negative for *KRAS* mutations, was the most frequent fusion among *KRAS* mutation-negative IMAs. Fusions of *CD74* or *SLC3A2* with *NRG1* were present in 17.6% (6/34) of cases. The five novel fusions were mutually exclusively with one another and were not present in any of the *KRAS* mutation-positive cases (Table 2).

Four of the novel fusions, *CD74-NRG1*, *SLC3A2-NRG1*, *EZR-ERBB4*, and *TRIM24-BRAF*, involved rearrangements of genes encoding protein kinases or a ligand of a receptor protein kinase (NRG1/neuregulin/heregulin) for which oncogenic rearrangements have not been previously reported in lung cancer (Supplementary Fig. S3). The remaining fusion was a novel type involving the *RET* oncogene; fusions with *RET* are observed in 1% to 2% of LADCs (4, 5, 7, 8, 11). In a screen of 315 LADCs without IMA features from Japanese patients and 144 consecutive LADCs from U.S. patients, all tumors were negative for all of the *NRG1*, *BRAF*, and *ERBB4* fusions, as well as the novel *RET* fusion. Therefore, these fusions might be driver aberrations specific to LADCs with IMA features. The four novel gene fusions were likely to have been caused by interchromosomal translocations or paracentric inversion (Table 1 and Supplementary Fig. S3). Consistently, separation of the signals generated by the probes flanking the translocation sites of *NRG1* in fusion-positive tumors was observed upon FISH analysis of *CD74-NRG1* fusion-positive tumors (Supplementary Fig. S4). We also confirmed overexpression of NRG1, ERBB4, and BRAF proteins in tumor cells carrying the corresponding fusions by immunohistochemical analysis, using antibodies recognizing polypeptides retained in the fusion proteins; expression of NRG1, ERBB4, and BRAF proteins was also observed in some fusion-negative cases (Supplementary Fig. S5). IMAs harboring gene fusions were obtained from both male and female patients, although

Published OnlineFirst April 11, 2014; DOI: 10.1158/1078-0432.CCR-14-0107

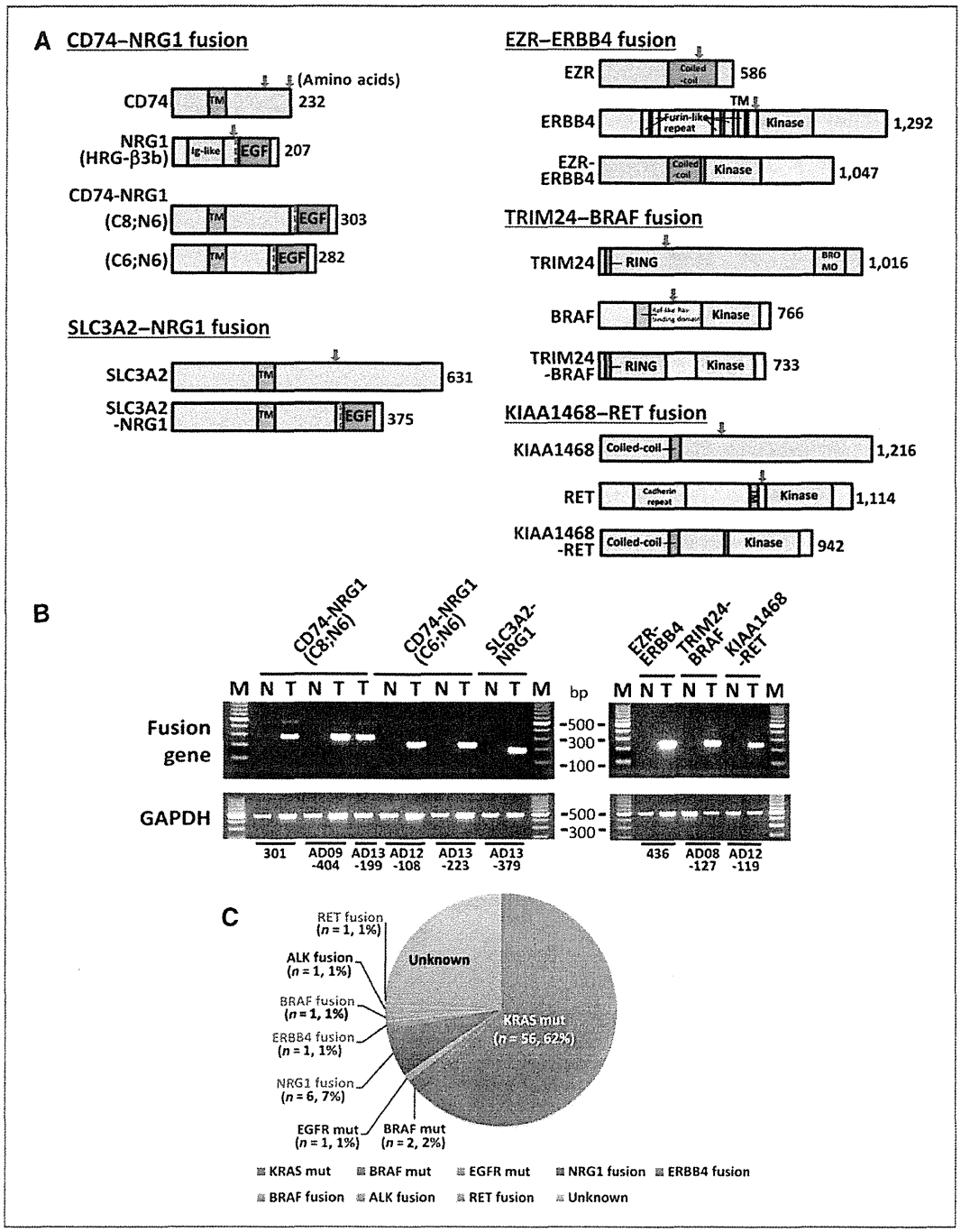

Figure 1. Oncogenic fusions in invasive mucinous LDAC. A, schematic representations of the wild-type proteins (top rows of each section) followed by the fusion proteins identified in this study. The breakpoints for each variant are indicated by blue arrows. TM, transmembrane domain. Locations of putative cleavage sites in the NRG1 polypeptide are indicated by dashed green lines. B, detection of gene-fusion transcripts by RT-PCR. RT-PCR products for glyceraldehyde-3-phosphate dehydrogenase (*GAPDH*) are shown below. Six IMAs (T) positive for gene fusions are shown alongside their corresponding non-cancerous lung tissues (N); labels below the gel image indicate sample IDs (see Table 1). C, pie chart showing the fraction of IMAs that harbor the indicated driver mutations.

Published OnlineFirst April 11, 2014; DOI: 10.1158/1078-0432.CCR-14-0107

Table 1. Characteristics of invasive mucinous LDACs with novel gene fusions

No.	Sample	Sex	Age	Smoking (pack/year)	Gene fusion	Chromosome aberration	Oncogene mutation[a]	Pathologic stage	TTF1	HNF4A
1	301T	M	55	Ever (47)	*CD74-NRG1*	t(5;8)(q32;p12)	None	1a	−	+
2	AD12-108T	F	68	Never	*CD74-NRG1*		None	2b	−	+
3	AD09-404T	F	78	Never	*CD74-NRG1*		None	1a	−	+
4	AD13-199T	F	47	Never	*CD74-NRG1*		None	1b	−	+
5	AD13-223T	F	53	Never	*CD74-NRG1*		None	1a	−	+
6	AD13-379T	F	66	Never	*SLC3A2-NRG1*	t(8;11)(p12;q13)	None	1b	Not tested	Not tested
7	436T	M	61	Ever (41)	*EZR-ERBB4*	t(2;6)(q25;q34)	None	1b	−	+
8	AD08_127T	F	66	Never	*TRIM24-BRAF*	inv7(q33;q34)	None	1a	+	+
9	AD12-119T	M	62	Current (63)	*KIAA1468-RET*	t(10;18)(q21;q11)	None	1a	+	−

[a]*EGFR*, *KRAS*, *BRAF*, and *HER2* mutations and *ALK*, *RET*, and *ROS1* fusions.

NRG1 fusion-positive cases were preferentially from female never smokers (Table 1).

The CD74-NRG1 and SLC3A2-NRG1 fusion proteins, whose sequences were deduced from RNA sequencing data, contained the CD74 or SLC3A2 transmembrane domain and retained the EGF-like domain of the NRG1 protein (NRG1 III-β3 form; Fig. 1A). The NRG1 III-β3 protein has a cytosolic N-terminus and a membrane-tethered EGF-like domain, and mediates juxtacrine signals signaling through HER2:HER3 receptors (19). Because parts of CD74 or SLC3A2 replaced the transmembrane domain of wild-type NRG1 III-β3, we speculated that the membrane-tethered EGF-like domain might activate juxtacrine signaling through HER2:HER3 receptors. In addition, it was also possible that expression of these fusion proteins resulted in the production of soluble NRG1 protein due to proteolytic cleavage at sites derived from NRG1 (dashed green lines in Fig. 1A), as recently suggested for NRG1 type III proteins (20, 21). Exposing EFM-19 cells to conditioned media from H1299 human lung cancer cells expressing exogenous CD74-NRG1 fusion protein resulted in phosphorylation of endogenous ERBB2/HER2 and ERBB3/HER3 proteins, suggesting that autocrine HER2:HER3 signaling was activated by secreted NRG1 ligands generated from CD74-NRG1 polypeptides (Fig. 2A). Phosphorylation of extracellular signal—regulated kinase (ERK) and AKT, downstream mediators of HER2:HER3, was also elevated. HER2, HER3, and ERK phosphorylation was suppressed by lapatinib and afatinib, U.S. Food and Drug Administration (FDA)-approved tyrosine kinase inhibitors (TKI) that target HER kinases (22–24). Together, these observations indicate that *NRG1* fusions activated HER2:HER3 signaling by juxtacrine and/or autocrine mechanisms.

The EZR-ERBB4 fusion protein contained the EZR coiled-coil domain, which functions in protein dimerization, and also retained the full ERBB4 kinase domain (Fig. 1A). These features indicated that the EZR-ERBB4 protein is likely to form a homodimer via the coiled-coil domain of EZR, causing aberrant activation of the kinase function of ERBB4, similar to the situation of *EZR-ROS1* fusion (5). Indeed, when the *EZR-ERBB4* cDNA was exogenously expressed in NIH3T3 fibroblasts, tyrosine 1258, located in the activation loop of the ERBB4 kinase site, was phosphorylated in the absence of serum stimulation, indicating that fusion with EZR aberrantly activated the ERBB4 kinase (Fig. 2B). Consistent with this, phosphorylation of a downstream

Table 2. Characteristics of 90 invasive mucinous LDACs

		Mutation			Fusion				
Variable	All	*KRAS*	*BRAF*	*EGFR*	*CD74-NRG1 or SLC3A2-NRG1*	*EZR-ERBB4*	*TRIM24-BRAF*	*EML4-ALK*	*KIAA1468-RET*	None (%)
Total	90 (100)	56 (62.2)	2 (2.2)	1 (1.1)	6 (6.7)	1 (1.1)	1 (1.1)	1 (1.1)	1 (1.1)	21 (23.3)
Age (mean ± SD; y)	67.2 ± 9.7	68.1 ± 9.7	66.5 ± 3.5	50	61.2 ± 11.5	61	66	64	62	68.1 ± 9.6
Sex										
Male (%)	39 (43.3)	28 (50.0)	0 (0)	0 (0)	1 (16.7)	1 (100)	0 (0)	0 (0)	1 (100)	8 (38.1)
Female (%)	51 (56.7)	28 (50.0)	2 (100)	1 (100)	5 (83.3)	0 (0)	1 (100)	1 (100)	0 (0)	13 (61.9)
Smoking habit										
Never smoker (%)	51 (56.7)	29 (51.8)	2 (100)	1 (100)	4 (66.7)	0 (0)	1 (100)	1 (100)	0 (0)	13 (61.9)
Ever smoker (%)	39 (43.3)	27 (48.2)	0 (0)	0 (0)	2 (33.3)	1 (100)	0 (0)	0 (0)	1 (100)	8 (38.1)

Published OnlineFirst April 11, 2014; DOI: 10.1158/1078-0432.CCR-14-0107

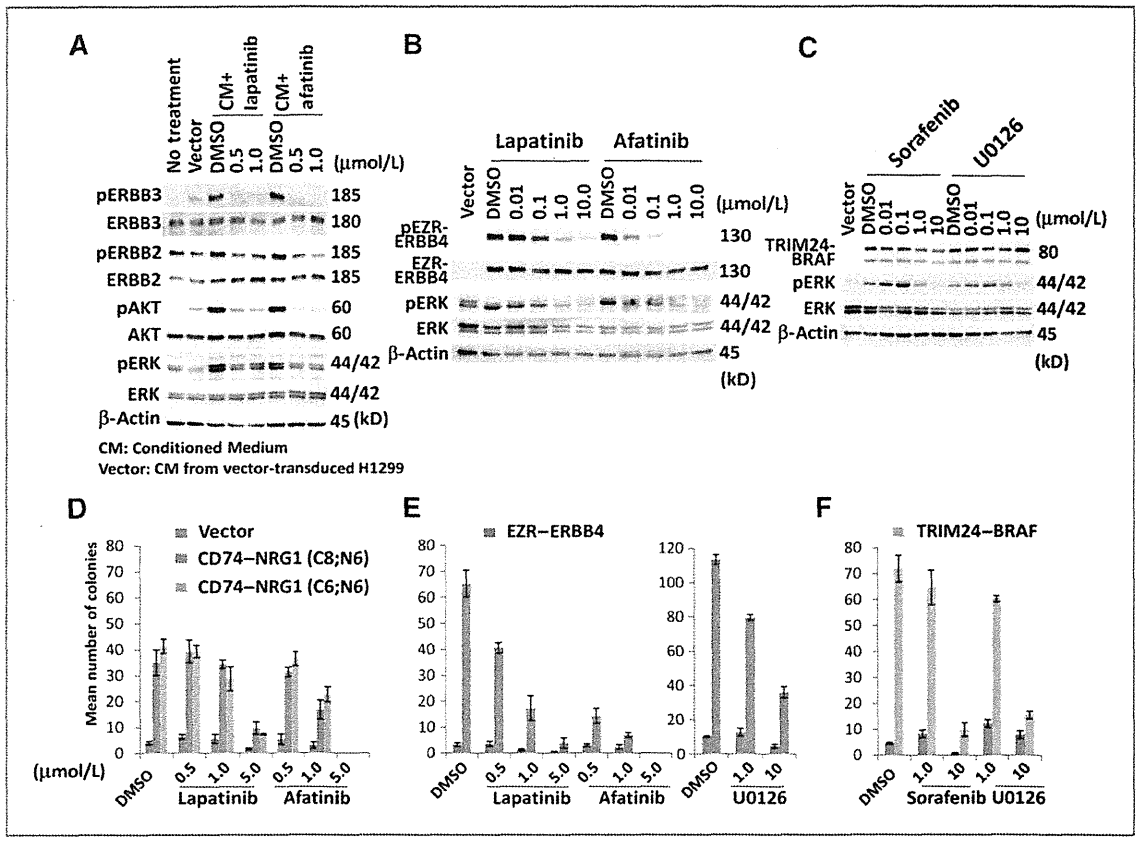

Figure 2. Oncogenic properties of gene-fusion products. A, ERBB3 activation by *CD74-NRG1* fusion, demonstrated using the EFM-19 cell system. ERBB3, ERBB2, AKT, and ERK phosphorylation were examined in EFM-19 (reporter) cells treated for 30 minutes with conditioned media from H1299 cells exogenously expressing *CD74-NRG1* cDNA. Phosphorylation was suppressed by HER-TKIs. B, ERBB4 activation by *EZR-ERBB4* fusion. Stably transduced NIH3T3 cells were serum-starved for 24 hours and treated for 2 hours with DMSO (vehicle control) or TKIs. Phosphorylation of ERBB4 and ERK was suppressed by ERBB4-TKIs. EZR-ERBB4 protein was detected using an antibody recognizing ERBB4 polypeptides retained in the fusion protein. C, BRAF activation by *TRIM24-BRAF* fusion. Stably transduced NIH3T3 cells were serum-starved for 24 hours and treated for 2 hours with DMSO or kinase inhibitors. ERK phosphorylation (activation) was suppressed by sorafenib, a kinase inhibitor targeting BRAF, as well as by U0126, a MEK inhibitor. TRIM24-BRAF protein was detected using an antibody recognizing BRAF polypeptides retained in the fusion protein. D–F, anchorage-independent growth of NIH3T3 cells expressing *CD74-NRG1* (D), *EZR-ERBB4* (E), or *TRIM24-BRAF* (F) cDNA, and suppression of this growth by kinase inhibitors. Mock-, *CD74-NRG1*-, *EZR-ERBB4*-, and *TRIM24-BRAF*–transduced NIH3T3 cells were seeded in soft agar with DMSO alone or kinase inhibitors. Colonies > 100 μm in diameter were counted after 14 days. Column graphs show mean numbers of colonies ± SEM.

mediator ERK was also elevated. Phosphorylation of ERBB4 and ERK was suppressed by lapatinib and afatinib, which inhibit ERBB4 protein (22–24).

The TRIM24-BRAF fusion protein retained the BRAF kinase domain but lacked the N-terminal RAS-binding domain responsible for negatively regulating BRAF kinase. These features suggested that the fusion was constitutively active, as in the cases of the *ESRP1-BRAF* and *AGTRAP-BRAF* fusions in other cancers (25). When the *TRIM24-BRAF* cDNA was exogenously expressed in NIH3T3 cells, ERK, a downstream mediator of BRAF, was phosphorylated in the absence of serum stimulation, indicating that fusion with TRIM24 aberrantly activated BRAF kinase (Fig. 2C). ERK phosphorylation was suppressed by sorafenib, an FDA-approved drug originally identified as a RAF kinase inhibitor (26), and also by the MEK inhibitor U0126 (Fig. 2C).

Exogenous expression of fusion gene cDNAs induced anchorage-independent growth of NIH3T3 fibroblasts, indicating their transforming activities (Fig. 2D–F). This growth was suppressed by the kinase inhibitors that suppressed fusion-induced activation of signal transduction, as described above. NIH3T3 cells expressing *EZR-ERBB4* or *TRIM24-BRAF* fusion cDNA formed tumors in nude mice (Fig. 3). Therefore, we concluded that these three fusions function as driver mutations in IMA development. We screened 200 commonly used human lung cancer cell lines, but all were negative for these three fusions (data not shown); thus, the oncogenic properties of these fusions remain unvalidated in human cancer cells.

Published OnlineFirst April 11, 2014; DOI: 10.1158/1078-0432.CCR-14-0107

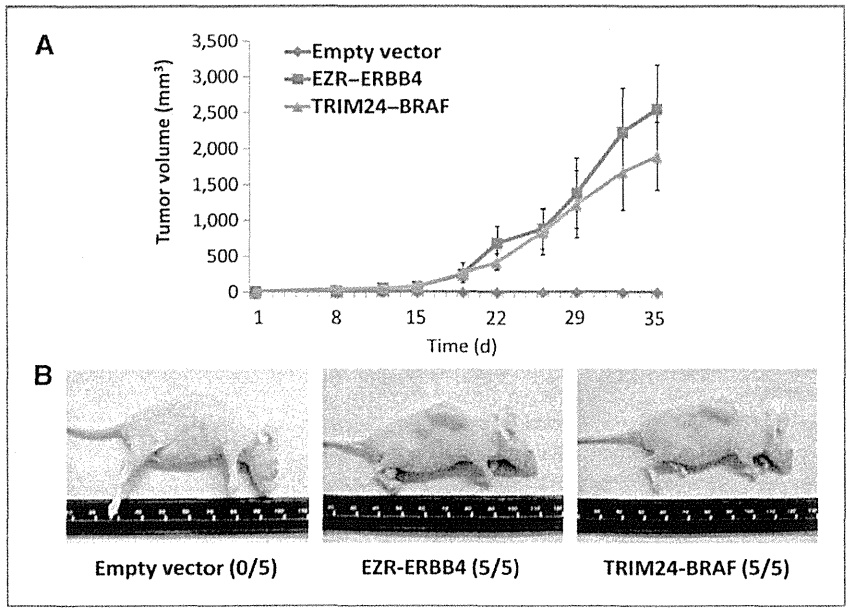

Figure 3. Tumorigenicity of NIH3T3 cells expressing *ERZ-ERBB4* or *TRIM24-BRAF* fusion cDNAs. A, tumor growth in nude mice injected with NIH3T3 cells expressing empty vector, *EZR-ERBB4* fusion, or *TRIM24-BRAF* fusion. Cells were resuspended with 50% Matrigel and injected into the right flank of nude mice. Tumor size was measured twice weekly for 5 weeks. Data are shown as mean ± SEM. B, representative tumors were photographed on day 21. The numbers in parentheses indicate the ratio of the number of mice with tumors to the number of mice receiving cell injection.

The results here suggest that the *NRG1*, *ERBB4* and *BRAF* fusions are novel driver mutations involved in the development of IMAs of the lungs (Fig. 1C) and potential targets for existing TKIs. The recurrent *NRG1* fusions were especially notable because NRG1 was previously identified as a regulator of goblet-cell formation in primary cultures of human bronchial epithelial cells (27); therefore, activation of the NRG1-mediated signaling pathway (s) might play a part in IMA development by contributing to both cell transformation and acquisition of goblet-cell morphology. In addition to a small fraction of known druggable aberrations (an *ALK* fusion and an *EGFR* mutation), more than 10% (11/90; 12.2%) of IMAs harbored other druggable aberrations targeted by existing kinase inhibitors: these aberrations were represented by fusions involving *NRG1*, *ERBB4*, *BRAF*, or *RET*, or *BRAF* mutations (Table 2, Fig. 1C). To facilitate translation of these findings to the cancer clinic, it will be necessary to establish diagnostic methods, particularly using break-apart and fusion FISH methods, capable of detecting these aberrations. Such methods will also help identify additional fusions involving other partner genes and contribute to a greater understanding of the significance of gene fusions in lung carcinogenesis.

Disclosure of Potential Conflicts of Interest

No potential conflicts of interest were disclosed.

Authors' Contributions

Conception and design: K. Tsuta, J. Yokota, T. Yoshida, T. Kohno
Development of methodology: H. Ichikawa
Acquisition of data (provided animals, acquired and managed patients, provided facilities, etc.): T. Nakaoku, K. Tsuta, H. Ichikawa, H. Sakamoto, K. Furuta, Y. Shimada, S.-I. Watanabe, H. Nokihara, K. Yasuda, M. Hiramoto, T. Nammo, T. Ishigame, H. Okayama
Analysis and interpretation of data (e.g., statistical analysis, biostatistics, computational analysis): T. Nakaoku, K. Tsuta, M. Enari, A.J. Schetter, C.C. Harris
Writing, review, and/or revision of the manuscript: T. Nakaoku, K. Tsuta, H. Ogiwara, S.-I. Watanabe, H. Nokihara, K. Yasuda, M. Hiramoto, A.J. Schetter, C.C. Harris, Y.H. Kim, M. Mishima, T. Yoshida, T. Kohno
Administrative, technical, or material support (i.e., reporting or organizing data, constructing databases): K. Tsuta, K. Shiraishi, M. Enari, H. Ogiwara, S.-I. Watanabe, H. Okayama
Study supervision: K. Tsuta, J. Yokota

Acknowledgments

The authors thank Suenori Chiku and Hirohiko Totsuka for the analysis of sequencing data and Dai Suzuki, Kazuko Nagase, Sachiyo Mitani, Sumiko Ohnami, Yoko Odaka, and Misuzu Okuyama for technical assistance.

Grant Support

This work was supported, in part, by the Advanced Research for Medical Products Mining Program of the National Institute of Biomedical Innovation (NIBIO), Grants-in-Aid from the Ministry of Health, Labor, and Welfare for the Third-term Comprehensive 10 year Strategy for Cancer Control and for Research for Promotion of Cancer Control Programs; and the Princess Takamatsu Cancer Research Fund.

The costs of publication of this article were defrayed in part by the payment of page charges. This article must therefore be hereby marked *advertisement* in accordance with 18 U.S.C. Section 1734 solely to indicate this fact.

Received January 14, 2014; revised March 22, 2014; accepted April 1, 2014; published OnlineFirst April 14, 2014.

References

1. Pao W, Hutchinson KE. Chipping away at the lung cancer genome. Nat Med 2012;18:349–51.
2. Shaw AT, Engelman JA. ALK in lung cancer: past, present, and future. J Clin Oncol 2013;31:1105–11.
3. Gautschi O, Zander T, Keller FA, Strobel K, Hirschmann A, Aebi S, et al. A patient with lung adenocarcinoma and RET fusion treated with vandetanib. J Thorac Oncol 2013;8:e43–4.